Evidence for a complex accretionary history preceding the amalgamation of Columbia: The Rhyacian Minas-Bahia Orogen, southern São Francisco Paleocontinent, Brazil

Henrique Bruno[1,2], Monica Heilbron[1], Claudio de Morisson Valeriano[1,3], Rob Strachan[2], Mike Fowler[2], Samuel Bersan[1], Hugo Moreira[2], Rafael Motta[4], Julio Almeida[1], Rasec Almeida[1], Mariana Carvalho[1,2], Craig Storey[2]

[1] – Universidade do Estado do Rio de Janeiro, Faculdade de Geologia, Tektos – Grupo de Pesquisa em Geotectônica. Rua São Francisco Xavier 524, Maracanã, Rio de Janeiro, Brazil.

[2] – University of Portsmouth, School of the Environment, Geography and Geosciences, Burnaby Building, Burnaby Road, Portsmouth, PO1 3QL, UK.

[3] – Laboratório de Geocronologia e Isótopos Radiogênicos, Universidade do Estado do Rio de Janeiro, Rua São Francisco Xavier 524, Maracanã, Rio de Janeiro, Brazil.

[4] – Departamento de Geologia, Centro de Ciências Exatas e da Terra, Universidade Federal do Rio Grande do Norte, Natal, RN 59078-970, Brazil.

Highlights

. Diachronous Collision of the São Francisco Paleocontinent

. Protracted orogenic cycle, from pre-subduction to late orogenic collapse is recognized within the Minas-Bahia Orogen

. A large continental landmass amalgamated during the Rhyacian (ca. 2.1-2.05 Ga)

. Archean-Paleoproterozoic basement units reworked during the Brasiliano Orogeny

Keywords:

São Francisco Craton, TTG-Sanukitoid, Orogenic collapse, Ribeira Belt, Columbia Supercontinent

Abstract

The Minas-Bahia orogeny juxtaposed Archean crustal fragments and Paleoproterozoic magmatic arcs to form the São Francisco-Congo Paleocontinent by the Rhyacian (ca. 2.05 Ga). Unravelling the Minas segment of the Minas-Bahia Orogenic Belt (MBO) is an important key to understanding the role of the São Francisco-Congo Paleocontinent in the construction of the Columbia Supercontinent. The Orosirian (ca. 1.9 Ga) final amalgamation of Columbia was preceded by a complex history of accretion of Archean nuclei and Proterozoic magmatic arcs. We present new whole-rock element geochemistry and isotopic (Rb-Sr, Sm-Nd) data and U-Pb ages for granitoid rocks of the main basement complexes located in the southern part of the São Francisco cratonic tip, which displays varied degrees of Neoproterozoic reworking related to the Brasiliano orogeny. Published data for the Campo Belo Complex, the Mineiro Belt and the Piedade Block are combined with the new data set to propose an integrated model for the tectonic evolution of the Minas segment of the MBO. This evolutionary model documents a complete Paleoproterozoic orogenic cycle, from subduction with terrane accretion to collision, followed by late-orogenic collapse. Subduction started diachronously between ca. 2.4 Ga and 2.2 Ga involving various Archean nuclei and Paleoproterozoic magmatic arcs that were later amalgamated during two collisional events at ca. 2.10 and 2.05 Ga. The oldest tonalite-trondhjemite-granodiorite (TTG) to sanukitoid magmatic suites transition are of Neoarchean age in the Piedade block, and of Paleoproterozoic age in the Mineiro belt and Mantiqueira complex, apparently indicating a diachronous onset of plate tectonic processes in different crustal segments. The petrogenesis, geochronology and isotopic signatures of these granitoid rocks provide important evidence towards understanding the periodicity of tectonic processes associated with the supercontinent cycle throughout Earth history.

1. Introduction

Magmatic rocks typical of the Archean (> 2.5 Ga) and Paleoproterozoic (2.5 to 2 Ga), such as tonalite-trondhjemite-granodiorite (TTG) association, sanukitoid and K-rich granites, are considered key indicators of the tectonic mechanisms that took place during early Earth history (e.g. Sun et. al., 2020; Laurent et. al., 2019; Moyen & Laurent, 2018; Rajesh et. al., 2018; Laurent, et. al., 2014; Moyen & Martin, 2012; Næraa et. al., 2012; Heilimo et. al., 2010; Halla et. al., 2009). The petrogenesis, geochronology and isotopic signatures of these granitoid rocks provide important evidence towards understanding the periodicity of tectonic processes associated with the supercontinent cycle throughout Earth history.

Various geochemical, isotopic and geochronological proxies can be used to determine the geodynamic settings of contrasting tectono-stratigraphic terranes and hence to develop tectonic models for the episodic assembly and break-up of supercontinents (Nance, 2019; Murphy & Nance, 2012; Condie, 2011; Hawkesworth et. al., 2010; Santosh & Zhao, 2009; Rogers & Santosh, 2002; Zhao, et. al., 2002).

The existence of the Columbia supercontinent during Paleo- and Mesoproterozoic times has been proposed with basis on paleomagnetic data as well as geological links between different continental blocks (e.g. Caxito et. al., 2020b; D'Agrella-Filho et. al., 2020; Iaccheri & Bargas, 2020; Wu et. al., 2020; D'Agrella-Filho & Cordani, 2017; Meert & Santosh, 2017; Xu et. al., 2014; Condie, 2013). Though the reconstruction of Archean and Proterozoic supercontinents is challenging due to the incomplete geologic record and reworking during later orogenic processes, their recognition can aid understanding of tectonic processes and mantle dynamics in those ages (e.g. Cawood et. al., 2016; Heron

et. al., 2015; Cawood & Buchan, 2007; Collins & Pisarevsky, 2005; Lowman & Jarvis, 1995).

The Paleoproterozoic orogenic belts of Brazil have crucial role in reconstructive models of the Columbia supercontinent, through the convergence and amalgamation of older, Archean continental fragments and new crust accretion through subduction. These orogenic belts are exposed both within the major cratons, such as the São Francisco, and as reworked basement inliers within the surrounding Neoproterozoic orogens. One of the most studied Paleoproterozoic orogenic belts, and focus of this work, is the Minas-Bahia Orogen (MBO), with the northern (Bahia) and southern (Minas) segments (Figure 1b).

The tectonic evolution of the MBO in the southern São Francisco Craton is reasonably constrained by a host of new data recently produced, as recently summarized by Teixeira et. al. (2017a). For a better understanding of this important Paleoproterozoic orogen as a whole, we present new geochemical, U-Pb geochronological, and isotopic Rb-Sr and Sm-Nd data from the basement inliers within the adjacent Neoproterozoic orogenic systems (Figure 1). We also propose new correlations with other cratonic blocks involved in the assembly of the Columbia supercontinent, e.g. the North China block, indicating a diachronous onset of plate tectonic processes in different crustal segments.

2. Tectonic Framework of the São Francisco Paleocontinent

The São Francisco-Congo Craton comprises various Paleoproterozoic orogenic belts and Archean nuclei that were largely unaffected by Neoproterozoic reworking during the west Gondwana supercontinent assembly (Figure 1a, b) (Alkmim & Teixeira, 2017; Caxito et. al., 2017; Teixeira et. al., 2017a; Valeriano et. al., 2017). However, these Neoproterozoic orogens contain slivers of reworked Paleoproterozoic and Archean basement associations that are comparable in most respects to those within the São Francisco-Congo Craton.

(Alkmim & Teixeira, 2017; Heilbron et. al., 2017b; Alkmim et. al., 2017) (Figure 1b). We therefore refer to the broader São Francisco Paleocontinent, which incorporates all the Archean and Paleoproterozoic units (Figure 1b).

The northern portion of the São Francisco Paleocontinent comprises a number of tectono-stratigraphic terranes that were diachronously amalgamated during the Minas-Bahia Orogeny (MBO): the Archean Gavião and Jequié blocks; the Paleoproterozoic Itabuna-Salvador-Curaçá Belt, characterized by both recycled and juvenile crustal additions; and the mainly juvenile Paleoproterozoic Buerarema Complex (Bersan et al., 2018; Aguilar et al., 2017; Barbosa & Barbosa, 2017; Cruz et al., 2016; Silva et al., 2016; Barbosa & Sabaté, 2004; Silva et al., 2002; Brito Neves et al., 1999; Oliveira et al., 2010) (Figure 1b).

The southern (Minas) segment of the MBO (Figure 2) comprises Paleoproterozoic magmatic arcs and the Archean Piedade block that were accreted to the northwest onto a large Archean TTG-greenstone belt crustal domain (Bruno et. al., 2020; Cutts, et. al., 2020; Degler et. al., 2018; Albert et. al., 2016; Barbosa et. al., 2015; Teixeira et. al., 2015; Goulart et. al., 2013; Lana et. al., 2013; Heilbron et. al., 2010, Duarte et. al., 2004; Teixeira et. al., 2000, Teixeira et. al., 1996) (Figure 1b).

3. Geological Context of the Study Area

The study area comprises basement inliers exposed in the external thrust-fold belts of the adjacent Neoproterozoic orogenic systems, represented in the west by the southern part of the ESE-verging Brasilia Belt (630-605 Ma) and in the east by the younger NW-verging (620 to 530 Ma) Ribeira Belt (eg. Heilbron et. al., 2017b, Trouw et. al., 2013; Valeriano et. al., 2008).

Broadly from northwest to southeast, the MBO comprises the following tectonic domains (Figure 2b):

i) a foreland domain where the Archean crust is better preserved from the Paleoproterozoic orogeny. It encompasses Meso- to Neoarchean gneissic-granitic greenstone terranes comprising TTG rocks, migmatites, K-rich granitoids, metaultramafic and supracrustal units (Figure 2b) covered by rift to passive margin basin, represented by the (2.6 – 2.1 Ga) Minas Supergroup, and syn- to post-collisional sedimentary successions (e.g. Teixeira et. al., 2017a; Farina et. al., 2015; Romano et. al., 2013; Lana et. al., 2013, Machado et al., 1996; Teixeira & Figueiredo, 1991);

ii) the Siderian to the Rhyacian accreted terrane, referred to as Mineiro Belt, consists of magmatic arc associations of juvenile to crustal contaminated high Ba-Sr, TTGs, sanukitoids, hybrid granitoid rocks and associated supracrustals (Araujo et al., 2019a; Cardoso et al., 2019; Moreira et al., 2018; Teixeira et al., 2015; Ávila et al., 2014; Seixas et al., 2013; Noce et al., 2000.);

iii) the accreted Piedade Block is interpreted as an Archean microcontinent, juxtaposed against the Mantiqueira Complex by the Ponte Nova Shear Zone, a Paleoproterozoic suture zone (Bruno et al., 2020; Peres et al., 2004). The rocks of the Piedade Block are Neoarchean TTGs and sanukitoids and associated mafic bodies, whose isotopic signatures indicates reworking of a pre-existing continental crust, and minor Paleoproterozoic granitoid rocks with post-collisional signatures (Bruno et al., 2020; Silva et al., 2002);

iv) and the Mantiqueira and Juiz de Fora complexes, both accreted Paleoproterozoic magmatic arcs (Bruno et al., 2020; Cutts et. al., 2020; Araújo et al., 2019b; Kuribara et. al., 2019; Degler et. al., 2018; Heilbron et. al., 2017b; Heilbron et.

al., 2010; Noce et. al., 2007; Duarte et. al., 2004; Silva et. al., 2002; Brueckner et. al., 2000). Geochemical and isotope data indicates juvenile to crustal contaminated granitoid rocks including TTGs, sanukitoids, post-collisional alkaline, within-plate tholeiitic basic rocks and peraluminous granitoid rocks with crystallization ages ranging from ca. 2.2 Ga to ca. 2.0 Ga, for the Mantiqueira Complex, and ca. 2.4 Ga to ca. 2.0 Ga, for the Juiz de Fora Complex (Figure 2b).

4. Field and Petrographic Features of the Sample Units

The studied basement units are reworked during the Neoproterozoic tectono-metamorphic event, which obliterated most of the primary textures. The metamorphic grade varies from green schist to high amphibolite facies with partial melting form the autochthonous towards the allochthonous domains of the studied area.

4.1 Piedade Block

In the studied outcrops of the Piedade Block, the most common lithology is a biotite orthogneiss with a well-developed metamorphic foliation, locally crosscut by layers of metabasic rocks (Figure 3a, b). The felsic biotite orthogneiss layers are dominated by inequigranular granoblastic texture, with quartz, plagioclase and K-feldspar and rounded mass intergrowths of epidote and clinozoisite, which might represent late replacement of plagioclase during epidote facies low-grade metamorphism (Figure 4a). The metabasic rock usually comprises metric to decametric layers of massive to finely banded metagabbro metamorphosed at epidote-amphibolite facies, with relict igneous clinopyroxene surrounded by coronas of poikiloblastic intergrowth between hornblende and quartz (Figure 4 b, c). Another lithotype is a muscovite -biotite granitoid. Biotite is scarce and related to coarse-grained muscovite crystals, defining a (proto)-mylonitic foliation (Figure 4 d, e). A well-foliated (hornblende)-biotite orthogneiss is also present,

with K-feldspar porphyroclasts (Figure 3c). Hornblende is rare and larger than the matrix and presents fine-grained inclusions of opaque minerals. It is often green-brownish in the core and green in the rim (Figure 4f), with late muscovite and chlorite. A banded orthogneiss with migmatitic textures characterized by hornblende-bearing leucosomes surrounded by hornblende-rich melanosomes, biotite and plagioclase is another lithotype (Figure 3d).

4.2 Campo Belo Complex

The main lithotype found in the Campo Belo Complex, within the Parautochthonous Domain is a medium-grained biotite orthogneiss (Figure 3e, f) It is characterized by biotite orthogneiss with the foliation defined by the orientation of brownish biotite. The texture is inequigranular, with microcline porphyroblasts, plagioclase is scarce, and quartz can be found in flaser textures. Titanite is subhedral and parallel to the main foliation (Figure 5a). Epidote occurs as coronas around plagioclase (Figure 5b). The granodioritic biotite orthogneiss main mineralogy is constituted by granular feldspars and quartz in the matrix, with the foliation defined by the orientation of biotite, late muscovite, and accessory epidote with allanite inclusions (Figure 5c, d).

4.3 Mineiro Belt

The main lithology of the Mineiro Belt found in the study area is a banded granodioritic hornblende-biotite orthogneiss with migmatitic textures, exposed in the Parautochthonous Domain (Sample 51B) (Figure 3g) and a granodioritic hornblende-biotite orthogneiss (Figure 3h) found in the Autochthonous Domain (Sample 42). In the Autochthonous domain it is mainly a coarse-grained metagranodiorite metamorphosed at greenschist facies. The main mafic mineral is a greenish biotite with no orientation. There are intergrowths between chlorite and zoisite, with the latter usually in coronas with spike

205 acicular texture (Figure 6a). Rutile interpreted as an igneous relict and always has coronas
206 of titanite that are interpreted as metamorphic (Figure 6b).The other variety found in the
207 Parautochthonous Domain of the Mineiro Belt shows a well-defined folded layering of
208 felsic and mafic bands, metamorphosed at epidote-amphibolite facies, where felsic bands
209 are dominated by granoblastic plagioclase and interstitial quartz, with minor K-feldspar,
210 and mafic layers are dominated by nematoblastic hornblende (Figure 6c) and biotite
211 oriented in the axial plane of the folds, defining a new foliation (Figure 6c). There are
212 some mafic bands where subhedral epidote is developed in the hornblende rims (Figure
213 6c, d) and titanite is fine- to medium-grained with subhedral texture (Figure 6d). Rutile
214 is rare and can be found included in titanite (Figure 6d).

215 **5. Analytical Methods**

216 Lithogeochemical, Laser Ablation Inductively Coupled Plasma Mass Spectrometry (LA-
217 ICPMS) U-Pb geochronology and thermal ionisation mass spectrometry (TIMS)
218 radiogenic isotope data were obtained from a range of samples from the Piedade Block,
219 the Campos Gerais Complex, and the Mineiro Belt. Major and trace elements composition
220 analyses, including rare-earth elements (REE) were carried out by Activation
221 Laboratories Ltd (Actlabs, Ancaster, Canada); the cathodoluminescence (CL) and
222 Backscattered electron (BES) imagery were performed in a Scanning Electron
223 Microscopy (SEM) at the School of the Environment, Geography and Geosciences
224 University of Portsmouth, UK; U-Pb data were obtained in the geochronology
225 laboratories of the University of Portsmouth (UK), and the Sm-Nd and Sr isotope data
226 were acquired by the Laboratory of Geochronology and Radiogenic Isotopes (LAGIR)
227 of the Rio de Janeiro State University (Brazil). The analytical procedures of the several
228 techniques and laboratories involved in this work can be found in Supplementary Material
229 A.

6. Results

6.1 Geochemistry

Fifteen samples were selected for major and trace element composition analyses (Supplementary Material B). Five compositional groups of acid and intermediate rocks (TTG, sanukitoid, hybrid, bitotite- two-mica and alkaline groups) and one compositional group of basic rocks (tholeiitic metabasic) have been discriminated based on their geochemical affinities.

6.1.1 TTG

Sample 50, from the Piedade Block, is characterized as silica-rich (71.8 wt.%), with high Na_2O contents (4.4 wt.%) and Na_2O/K_2O ratio (1,7), low Mg# (37) and is poor in ferromagnesian elements (Fe_2O_3 + MgO + MnO + TiO_2 = 3.7%). It plots on the calc-alkaline series on the AFM diagram (Figure 7a) and on the granite field on the SiO_2 vs. Na_2O+K_2O (TAS) diagram (Figure 7b). The sample is classified as slightly peraluminous ($1.0 \leq A/CNK \leq 1.1$), medium-K calc-alkaline rocks and magnesian (Figure 8a,b,c). It plots in the overlap field of different groups in the ternary diagram of Figure 8d. The TTG affinity, of this one sample, is corroborated by high concentrations of incompatible elements Ba (1365 ppm), Sr (459 ppm), low Y (6ppm), high Sr/Y ratio (76.5), and low concentrations (under detection limit $\leq$ 20 ppm) of compatible trace elements (Ni, Cr). In the REE chondrite-normalized diagram, it shows enrichment of light rare earth elements (LREE) compared to the heavy rare earth elements (HREE), with high $(La/Yb)_N$ (106) and positive Eu anomalies (Eu/Eu* = 1.26; Figure 9a).In the primitive mantle diagram (Figure 9b), the sample has peaks at Ba, Pb and Zr and troughs at P, Nb and Ti.

6.1.2 Sanukitoids

253 The second compositional group comprises samples 42, 51B, 52A and 52B from the
254 Mineiro Belt. This group has SiO_2 contents varying from 60.32– 68.15 wt.% (Figure 7a)
255 and plots in the intermediate and acid field of the TAS diagram and on the calc-alkaline
256 series on the AFM diagram (Figure 7b). The samples have been classified as
257 metaluminous (Figure 8a), medium-K calc-alkaline rocks in the SiO_2 vs. K_2O diagram
258 (Figure 8b), magnesian (Figure 8c) and sanukitoids in the ternary diagram 2*A/CNK vs.
259 Na_2O/K_2O vs. 2*FMSB (Figure 8d). They are rich in ferromagnesian oxides ($5 \leq FeOt +$
260 $MgO + MnO + TiO_2 \leq 25$ wt.%) and CaO. All have high concentrations of compatible
261 trace elements Ni (30-110 ppm), Cr (50-130 ppm) and V (60-152 ppm), in incompatible
262 elements (Ba = 430 – 1251 ppm and Sr = 236 - 1010 ppm), and high Mg# (47-58) for
263 their silica content, corroborating their sanukitoid classification. The chondrite-
264 normalized REE patterns show enrichment in LREE relative to HREE with moderate
265 $(La/Yb)_N$ (8 - 23) and slightly negative to positive Eu anomalies (Eu/Eu* = 0.98 – 1.11)
266 (Figure 9c). In the primitive mantle diagram, all the samples show enrichment in large
267 ion lithophile elements, with peaks in Ba, K, Pb and Sr and troughs at P, Ti, and Nb
268 (Figure 9d).

269 **6.1.3 Biotite-/Two-Mica Granitoids**

270 Samples 65, 68A, 69A and 70B, from the Piedade Block, comprise the third
271 compositional group. They are characterized by high silica contents (SiO_2> 71.95 wt.%),
272 low concentrations of ferromagnesian oxides ($FeO_t+MgO+MnO+TiO_2 \leq$ 4 wt.%) and
273 CaO (< 3 wt.%), moderate Al_2O_3 (13.55 $\leq Al_2O_3 \leq$15.05 wt.%) leading to high
274 Al_2O_3/(FeOt+MgO). They plot on the calc-alkaline series (Figure 7a) and on the granite
275 field on the TAS diagram (Figure 7b). They have peraluminous affinity (A/CNK $\geq$1),
276 medium to high-K calc-alkaline signatures and plot in the magnesian field of the SiO_2 vs.
277 FeO_t / (FeOt + MgO) diagram (Figure 8a, b, c). In the ternary diagram of Laurent et al.,

(2014), the samples plot on the Biotite- Two-mica granites (Figure 8d. The samples have low high field strength elements (HFSE) and transition element contents (such as Zr and V) and Ba/Rb and Sr/Y ratios. REE chondrite-normalized diagram show moderate fractionation of REE patterns (10.11 $\leq$LaN/Yb$_N$ $\leq$36.81) but significant negative Eu anomalies (Eu$_N$/Eu* = 0.25–0.71) (Figure 9e). The primitive mantle diagram (Figure 9f) shows high contents in highly incompatible elements such as Rb and Th.

6.1.4 Hybrid Granitoids

Samples 58B, from the Piedade Block, and 48A and48B from the Campo Belo Complex, plot on the calc-alkaline series (Figure 7a) and have high SiO_2 (wt. 69.15-71.02%), therefore they plot on the granite field on the SiO_2 vs. Na_2O+K_2O diagram (Figure 7b). They have high Al_2O_3 (15.23-17.14%), moderate Na_2O (3.42-4.69%) and K_2O contents (2.52-3.63%; and therefore Na_2O/K_2O ratios, ranging from 0.94-1.86), and low MgO (0.09-0.79%), Cr and Ni (below detection limits) contents are also characteristic of the compositional group. They are peraluminous, medium to high-K calc-alkaline rocks and straddle the ferroan and magnesian fields of the SiO_2 vs. FeO_t / (FeOt + MgO) diagram (Figure 8a, b, c). In the petrogenetic indicator ternary diagram (Figure 8d), the samples plot in the hybrid granites field, reflecting a mixed parentage, likely a mix of felsic magmas and crustal melts (Laurent et al., 2014). The REE chondrite-normalized diagram (Figure 9g) shows enrichment of LREE relative to HREE, with moderate to high (La/Yb)$_N$, ranging from 15.5 to 209. The samples also have slightly negative to positive Eu anomalies (Eu$_N$/Eu* = 0.71–2.15), high Sr (400 to 508 ppm) and low Y (<1 to 6 ppm) contents, resulting in high Sr/Y ratios of 68–400 (obs.: the higher value of 400 is a minimum estimation, since Y concentration in sample 58B is below the detection limit). In mantle-normalized trace element diagrams (Figure 9h), they are characterized by

enrichment of LILE (large-ion lithophile elements), depletion of Nb and Ta, and positive Pb and negative Ti anomalies.

6.1.5 Alkaline Rock

Sample 58A from the Piedade Block is significantly different, as it displays high contents of K_2O (5.08 wt.%) and other incompatible elements (Ba 5729 ppm, Sr 1235 ppm) together with a low Na_2O/K_2O ratio (0.73). In the AFM diagram it plots on the calc-alkaline series, however on the TAS diagram, the sample straddles the subalkaline and alkaline series (Figure 7 a, b). It has high contents of Zr, Nb, Ce and Y corroborating its alkaline signature. Chondrite-normalized REE patterns show high LREE and low HREE, leading to a highly fractionated REE pattern ($La_N/Yb_N \leq 232.97$) and a small negative Eu anomaly ($Eu_N/Eu^* = 0.93$) (Figure 9i). In the primitive mantle diagram, there is clear enrichment in LILEs (Ba, Rb and K) and a negative Ti anomaly (Figure 9j).

6.1.6 Tholeiitic Metabasic Rocks

The metabasic rocks of the study area, represented by samples 68B and 70A from the Piedade Block, are considered as one compositional group. All samples are classified as tholeiitic in an AFM diagram (Figure 7a) and, on the TAS diagram (Figure 7b), they plot on the subalkaline/tholeiitic series. Chondrite-normalized REE shows a flat pattern ($1.32 \leq La_N/Yb_N \leq 1.39$) and small negative to absent Eu anomalies ($0.97 \leq Eu_N/Eu^* \leq 1$), indicating an E-MORB (enriched mid-ocean ridge basalts) signature (Figure 10a). They have low TiO_2 (wt.% <2), moderate Mg# (51-52), high contents of CaO, Al_2O_3, and therefore high Al_2O_3/TiO_2 ratios. In the N-MORB-normalized diagram (Figure 10b), despite the metamorphism, the group shows signs of enrichment in incompatible elements such as K, B, La and Rb peaks at Ba, K, Pb and Nd. In the tectonic discriminant diagram

of Meschede (1986; Figure 10c) the samples plot in the N-type MORB field. In the Zr vs. Ti diagram of Pearce (1982; Figure 10d), the samples also plot in the MORB field.

6.2 U-Pb Geochronology

Following geochemical analysis, zircon LA-ICPMS U-Pb geochronology data were obtained from twelve samples which covered the range of different geochemical signatures across a wide geographical area, including the Piedade Block, the Mineiro Belt and the Campo Belo Complex (Figure 2). Tables with analytical results are provided in Supplementary Material C.

6.2.1 Piedade Block

The results of sample 50, a hornblende biotite gneiss from the TTG compositional group from the Piedade Block (Figure 2), are complex with thirty-six analyses of zircon cores and rims arranged into two discordia lines. (Figure 11a). The most common zircon morphology is prismatic (subhedral), with rounded grains, that display fine igneous oscillatory zoning in the cores surrounded by homogeneous bright and dark rims. The first discordia line defined by cores with fine igneous oscillatory zoning and dark metamorphic rims yielded an upper intercept of 2776 ± 28 Ma and a lower intercept of 1930 ± 37 Ma (Figure 11a). Six analysis of cores yielded a concordia age of 2691± 18 Ma, interpreted as the crystallization age (Figure 11b); the analysis of the dark rims in the spots#20 and #34, with 98% and 99% of concordance, yielded $^{207}Pb/^{206}Pb$ age of 2021 ± 30 Ma and 2043 ± 29 Ma, respectively, and are interpreted as metamorphic ages. The second discordia line, defined by cores with fine igneous oscillatory zoning and bright metamorphic rims, yielded an upper intercept of 2705 ± 13 Ma and a lower intercept of 592 ± 44 Ma (Figure 11a). Three analyses of the bright metamorphic rims yielded a concordia age of 578± 3 Ma, interpreted as the Neoproterozoic metamorphic overprint (Figure 11c).

Zircon grains from Sample 65, a felsic orthogneiss of the biotite- two-mica compositional group collected close to the Ponte Nova Shear Zone (Figure 2), are prismatic to subhedral displaying inherited cores, fine igneous oscillatory zoning, and bright metamorphic rims. Eighteen analyses define a discordia with an upper intercept of 2011 ± 30 Ma and a lower intercept of 540 ± 27 Ma, interpreted as igneous crystallization and metamorphic overgrowth ages, respectively (Figure 11d). The analysis of nine inherited cores are shown as blue ellipses in the concordia diagram and have $^{207}Pb/^{206}Pb$ ages from 2767 ± 9 Ma (spot #10) with Pb loss towards the Neoproterozoic metamorphic overprint. (Figure 11 d).

Sample 68A is also a biotite gneiss of the biotite- two-mica compositional group of the Piedade block (Figure 2). The most common morphology of the zircon grains is prismatic subhedral with fine igneous oscillatory zoning, sometimes showing inherited cores (Figure 11e). The grains are mostly fractured in the BSE images and are translucent to opaque with light to deep yellow colors. The analysis of an inherited core yielded a $^{207}Pb/^{206}Pb$ age of 2497 ± 36 Ma (spot #35). Thirteen analyses yield a discordia line with upper intercept at 2051 ± 30 Ma and lower intercept at 449 ± 44 Ma, the latter interpreted as Pb loss during Neoproterozoic metamorphism. Seven analyses yielded a concordia age of 2048 ± 28 Ma, interpreted as the igneous crystallization age (Figure 11e).

Sample 70A, a tholeiitic metabasic rock from the Piedade Block (Figure 2), displays translucent prismatic euhedral to subhedral, with a few rounded, zircon grains, varying from light to dark brown colours. Six discordant analyses of inherited cores show $^{207}Pb/^{206}Pb$ age of 2718 ± 14 Ma with 93% of concordance (spot #23) to $^{207}Pb/^{206}Pb$ age of 2458 ± 13 Ma with 90% of concordance (spot#6) (Figure 11f). Sixteen analysis of fine igneous oscillatory zoning of the prismatic grains yielded a concordia age of 2053 ± 18 Ma, interpreted as the crystallization age (Figure 11f).

375 Sample 70B, a biotite orthogneiss of the biotite- two-mica compositional group, collected
376 in the same outcrop of Sample 70A (Figure 2), has the most common morphology of the
377 zircon grains, namely prismatic subhedral showing cores and rims with igneous
378 oscillatory zoning (Figure 11g). The grains are commonly fractured in the BSE images
379 and mostly translucent with light to deep brown colors. Twenty core analyses scatter
380 along the Concordia, varying from a $^{207}Pb/^{206}Pb$ age of 2866 ± 35 Ma (spot #16; 98% of
381 concordance) to $^{207}Pb/^{206}Pb$ age of 2110 ± 44 Ma (spot #14; 91% of concordance) are
382 interpreted as inheritance ages. Four analyses (spots #11, #15, #20, #26) in zircon grains
383 with igneous oscillatory zoning yield a concordia age of 2059± 35 Ma, interpreted as the
384 crystallization age (Figure 11g).

385 Zircon grains from sample 58A, a hornblende biotite gneiss from the alkaline
386 compositional group from the Piedade Block (Figure 2), are rounded to subhedral with
387 fine igneous oscillatory zoning. Thirty-three analyses of concordant to sub concordant
388 grains vary from $^{207}Pb/^{206}Pb$ age of 2130 ± 31 Ma (spot #17) with 96% of concordance to
389 $^{207}Pb/^{206}Pb$ age of 2021 ± 32 Ma (spot #25) with 91% of concordance. The average
390 $^{207}Pb/^{206}Pb$ mean age of 2058 ± 6 Ma is within error of the upper intercept age of 2078 ±
391 6 Ma (all zircons) and interpreted as the crystallization age (Figure 12a).

392 Zircon grains from sample 58B, a biotite-muscovite orthogneiss from the hybrid granitoid
393 compositional group collected in the same outcrop of Sample 58A, are subhedral to
394 rounded, translucent to opaque brownish colors with oscillatory zoning in the cores and
395 bright metamorphic rims. Thirty-three analyses yield a discordia with an upper intercept
396 of 2054 ± 24 Ma, interpreted as the crystallization age, and a lower intercept of 538 ± 47
397 Ma, interpreted as indicative of the Neoproterozoic metamorphic overprint (Figure 12b).

398 **6.2.2 Mineiro Belt**

Sample 42, a metagranodiorite of the sanukitoid compositional group collected in the Autochthonous Domain (Figure 2), yielded an upper intercept of 2139 ± 40 Ma with the most common morphology of the zircon grains being prismatic subhedral with fine igneous oscillatory zoning (Figure 13a). The grains are mostly translucent with light to deep yellow colors. The average mean $^{207}Pb/^{206}Pb$ ages of the 32 analyses, with at least 95% of concordance, give an age of 2114 ± 10 Ma, interpreted as the crystallization age (Figure 13b).

Sample 51B was an amphibolitic gneiss of sanukitoid composition collected in the Parautochthonous Domain (Figure 2). Thirty analyses of subhedral to euhedral prismatic zircon grains, displaying fine igneous oscillatory zoned cores and bright rims yield an upper intercept of 2117 ± 24 Ma and a lower intercept of 551 ± 36 Ma, interpreted as crystallization and metamorphism ages, respectively (Figure 13c). Five discordant analyses of bright cores surrounded by igneous oscillatory zoning textures are interpreted as inheritance (Figure 13c).

Zircon grains from sample 52B, a hornblende biotite orthogneiss from the sanukitoid compositional group also collected in the basement thrust sheets of the Brasilia Belt (Figure 2), are mostly translucent, varying from light to dark yellow colours and euhedral to subhedral showing fine igneous oscillatory zoning in the cores and bright rims (Figure 13d). Sixty analyses yield a discordia line with an upper intercept of 2152 ± 11 Ma, interpreted as the crystallization age, and a lower intercept of 577 ± 32 Ma, interpreted as metamorphism related to Neoproterozoic orogeny (Figure 13d).

6.2.3 Campo Belo Complex

Zircon grains from sample 48A, a biotite gneiss from the hybrid granitoid compositional group of the Parautochthonous Domain (Figure 2), are prismatic, subhedral to euhedral,

and show dark cores surrounded by fine igneous oscillatory zoning textures and small bright rims (Figure 14b). The analyses of the cores are interpreted as inheritance, with $^{207}Pb/^{206}Pb$ ages from 3007 ± 90 Ma (spot #16; with 98% of concordance) to an age of 2621 ± 93 Ma (spot #4; with 88% of concordance). The analyses of the igneous oscillatory zoned areas and the bright rims yield a discordia line with an upper intercept of 2165 ± 39 Ma and a lower intercept of 585± 67 Ma, interpreted as corresponding to the ages of crystallization Neoproterozoic metamorphism, respectively (Figure 14b). Five analyses of concordant to sub concordant grains yielded a concordia age of 2090 ± 24 Ma, interpreted as a better constraint on the crystallization age of the rock (Figure 14b).

The results of sample 48B, a biotite gneiss of the hybrid compositional group collected in the same outcrop of Sample 48A (Figure 2), are complex with twenty-seven analyses of cores and rims in prismatic brownish zircon grains, showing dark cores and rims with igneous textures, being interpreted to correspond to inheritance and crystallization, respectively. The analysed cores show $^{207}Pb/^{206}Pb$ ages from of 2794 ± 36 Ma (spot #19; with 91% of concordance) to 2009 ± 53 Ma (spot #16; with 89% of concordance), being interpreted as inheritance, showing a Pb loss trend towards the Neoproterozoic (Figure 14c). Eighteen analyses of the rims yield a discordia line with upper intercept at 2096 ± 59 Ma, and a lower intercept of 931 ± 390 Ma, interpreted as the ages of crystallization and Neoproterozoic metamorphism, respectively.

6.3 Isotope data

Eleven samples were selected based on their geochemical affinities and different tectonostratigraphic terranes. Samples from the Piedade Block, Mineiro Belt and Campo Belo Complex show a wide variety of εNd(t) values, varying between juvenile (+1.3) to strongly evolved (-16), at their respective crystallization ages (Supplementary Material D). For sample 69, the crystallization age used for εNd(t) calculations was that obtained

for other samples from the same lithogeochemical group and tectonostratigraphic terrane. In the εNd(t) vs crystallization age diagram (Figure 15), the different isotopic fields of the Archean and Paleprotoerozoic terranes previously published for the studied area are shown in order to compare with the results obtained in this study.

The diversity of Initial $^{87}Sr/^{86}Sr$ and $^{143}Nd/^{144}Nd$ ratios, vary widely, from 0.700 to 0.788 and 0.5091 to 0.5107, and relate to the respective lithogeochemical group of the studied samples, despite their crystallization age. Lower initial $^{87}Sr/^{86}Sr$ correlated with the chondritic εNd(t), reproduces the mantle isotopic reservoir that originated the tholeiitic metabasic and sanukitoid groups, while the higher values of $^{87}Sr/^{86}Sr$ ratios are also correlated with negative εNd(t) values and likely represent reworking of pre-existing continental crust, represented by the biotite- two-mica and hybrid compositional group.

7. Discussions

7.1 Petrogenetic Implications

Combining isotopic information and whole-rock geochemistry of igneous rocks is a powerful tool for understanding igneous petrogenesis and related tectonic processes (Moyen, 2019; Laurent et. al., 2011), providing different petrogenetic scenarios for the studied lithogeochemical groups. The initial (t = U-Pb crystallization age) εNd vs. $^{87}Sr/^{86}Sr$ diagram of Figure 16 highlights the role of continental crust contamination in the generation of magmatic suites. In this context, different rock assemblages show varied degrees of mantle participation in their origins, from the least contaminated, mantle-derived TTG (Sample 50 of the Piedade Block) and sanukitoid (Samples 42, 51B and 52B of the Mineiro Belt) suites, to the more contaminated magmatic suites of hybrid, alkaline and biotite-bearing or two-mica granitoid rocks. Younger tholeiitic basic magmatism, represented by sample 70A, shows a subcontinental lithospheric mantle source (Figure 16).

The combination of initial (t = crystallization ages) εNd vs whole-rock element compositions confirm the varied degrees of mantle interaction of the aforementioned lithogeochemical groups (Figure 17 a, b). This is exemplified in the binary plot of #mg vs. initial εNd and of #mg vs. initial $^{87}Sr/^{86}Sr$. The highest εNd is correlated with the highest #mg, showing the mantellic signatures of the aforementioned rocks and the highest $^{87}Sr/^{86}Sr$ with the lowest #mg, indicating a more continental signatures for the samples.

The sanukitoid magmas were likely sourced from a fluid metasomatized mantle wedge, reinforcing recent studies about the repetition in time and space of this type of magmatism in the geological record, implying subduction of sediment followed by its interaction with the mantle wedge (Bruno et al., 2020; Laurent et. al., 2019; Moreira et. al., 2018, Laurent et. al., 2014). Remarkably, the samples show mantle affinity and isotopic signatures close to chondritic compositions (Figure 15) and in the Sr + Ba (ppm) vs. (FeOt+MgO wt.%) diagram (Figure 17c) the source of the sanukitoid group is characterized as the melting of enriched mantle. Among the Palaeoproterozoic sanukitoids, only one sample (51B) has a negative εNd value below -5, the other two (Sample 42, 52B) have a less evolved Nd signature. The latter probably reflects the involvement of coeval sediments (~2.1 Ga) acting as metasomatic agents in the mantle wedge. Furthermore, the first could be accounted for by an Archaean sedimentary contribution due to overlap with crustal arrays in the εNd space (Figure 16) and the presence of inherited zircon grains (Figure 13c). The Archean TTG (sample 50) shares the melting of enriched mantle (Figure 17c) of the sanukitoid suite and show elevated MgO, sharing the characteristics of the Low Al and High-HREE, what favors a geodynamic setting with shallow low-pressure source possibly with a mantle involvement (Halla et. al., 2009).

Samples of this study classified as two-mica granitoids have overall the lowest εNd values and the highest $^{87}Sr/^{86}Sr$ (initial). Because of the peraluminous geochemical affinity of these samples and low FeOt+MgO (wt.%), it is assumed that the samples generated by partial melting of crustal lithologies, therefore implying the presence of a significant sedimentary contribution to the protolith (Figure 17 c, d) (e.g. Bucholz et al., 2018). This interpretation is supported by the presence of inherited grains with a range of Paleoproterozoic and Archaean ages (Figure 11 d, e, g), likely sourced during partial melt of the mid-crust.

A distinct lithogeochemical group found in the study area is represented by the hybrid granitoids (Samples 48A and 48B of the Campo Belo Complex and Sample 58B of the Piedade Block) classified after the ternary diagram of Laurent et. al. (2014). They are classified as late- to – post-collisional and despite the relatively high K2O content, the chemical signatures of these rocks resembles those of adakitic rocks (high Na2O, Al2O3, Sr, Eu contents, low Yb and Y contents, enrichment in LREEs and LILEs and depletion in HREE, high Sr/Y and Na_2O/K_2O and La/Yb(N) ratios (Drummond and Defant, 1990, Martin et al., 2005). It is highlighted that their crystallization ages are different, ca. 2.10 Ga for samples 48A and 48B of the Campo Belo Complex and ca. 2.05 Ga of the Piedade Block, representing the same geological process at different times, since they are related to different collisional events.

Several models have been proposed for the petrogenesis of adakitic granitoids, including: (1) assimilation–fractional crystallization from a parental basaltic magma (Rooney et al., 2011; Castillo et al., 1999), (2) partial melting of a young subducted oceanic slab (Castillo, 2012; Martin et al., 2005), (3) partial melting of delaminated lower continental crust with mantle interaction (Wang et al., 2006; Xu et al., 2006; Gao et al., 2004; Kay and Kay, 2002; Xu et al., 2002), and (4) partial melting of thickened mafic lower crust

(Huang et al., 2009; Gao et al., 2004; Chung et al., 2003; Xiong et al., 2003; Kay and Kay, 2002; Atherton and Petford, 1993). The following observations with respect to the studied rocks seem pertinent. Although fractionation of garnet, amphibole and plagioclase from a basaltic magma could produce residual melts with adakitic compositions, our samples have narrow ranges of MgO and SiO_2. Thus, some form of direct generation by crustal partial melting is more likely the dominant process involved in the petrogenesis of these rocks. Low MgO, Mg#, Cr and Ni contents contrast with those expected for adakites derived from slab-derived magmas or delaminated lower continental crust with mantle interaction (Castillo, 2012; Martin et al., 2005). On the other hand, chemical and petrographic characteristics are indicative of high-pressure melting, with garnet and no plagioclase in the residue (as positive Sr, Eu anomalies, high Sr/Y ratio, low Y and Yb contents. Thus, the rocks presented here have affinities with adakites derived from thickened lower crust (Liu et. al., 2020).

The crystallization of the post-collisional granitoids can indicate a delamination of the lower crust and lithospheric mantle providing an asthenosphere inflow in a favorable configuration for melting, responsible for the bi-modal magmatism found in the Paleoproterozoic samples of Piedade Block (eg. Laurent et. al., 2019).

7.2 Southern São Francisco Paleocontinent Tectonic Model

Within the units of the São Francisco Paleocontinent, the ca. 2.4 to 2.07 Paleoproterozoic granitoid rocks with high Ba-Sr, sanukitoid and TTG signatures suggest a complex and diachronous subduction history (Bruno et. al., 2020; Cutts, et. al., 2020; Araújo et. al., 2019b; Moreira, et. al., 2018; Degler et. al., 2018; Heilbron et. al., 2017b; Teixeira et. al., 2015, Seixas et. al., 2013). Late- to post-collisional granitoid rocks between ca. 2.1 and 2.06 Ga and an important metamorphic record at ca. 2.05 to 2.04 Ga, with the development of associated foreland basins marked the final transition to extensional

collapse (Cutts, et. al., 2019; Alkmim & Teixeira, 2017; Aguilar Gil et. al., 2015; Vlach et. al., 2003; Brueckner et. al., 2000; Machado et. al., 1992) (Figure 18).

A complete orogenic cycle from subduction to collisional stages, followed by late orogenic lithospheric collapse with associated magmatism is recognized within the different tectono-stratigraphic terranes of the Minas segment of the MBO (Figure 18). Its Siderian-Rhyacian evolution, which led to the amalgamation of the São Francisco-Congo Paleocontinent, is characterised by the diachronous accretion of Archean blocks with cordilleran (e.g. Mantiqueira Complex) and intra-oceanic juvenile accretionary arcs (e.g. Mineiro Belt and Juiz de Fora Complex). Based on the geochronological, isotopic and lithogeochemical constraints we propose a tectonic model for the Minas-Bahia orogen. Available data for the Archean complexes of the southern São Francisco Paleocontinent show that Meso- and Neoarchean polycyclic terranes are mainly composed of TTG, migmatites and potassic granitoids suites (e.g. Alkmim & Teixeira, 2017). Based on description by Bruno et. al., (2020) and on the results of this study (Sample 50), the Neoarchean Piedade Block is composed of TTGs and sanukitoids, with subordinated within-plate alkaline basalts. The existence of an Archean microcontinent, represented by the Mantiqueira Complex, is indicated by the presence of Archean inherited zircon grains in Paleoproterozoic arc-related granitoid rocks (eg. Heilbron et. al., 2010) and by the Nd and Sr isotope signatures indicative of a mixed crust-mantle origin (Bruno et al., 2020).

From 2.4 to 2.1 Ga (Figure 19a), the crystallization of juvenile magmatic arc rocks of in the Mineiro Belt and of the granitoid rocks of the Juiz de Fora Complex, are interpreted to represent the early, accretionary stages of the southern portion of the MBO (Moreira et. al., 2018, Teixeira et al., 2017, Barbosa et. al., 2015; Ávila et. al., 2014; Ávila et. al., 2010, Heilbron et. al., 2010, Teixeira & Figueiredo, 1991).

As the magmatic arc system was constructed, an east-directed subduction system of ca. 2.2 – 2.1 Ga is interpreted as responsible for the generation of rocks with mixed mantle-crust isotopic signature in the Juiz de Fora Complex, and of coeval TTGs and sanukitoid suites in the Mineiro Belt (Samples 42, 51B and 52B) and Mantiqueira Complex (e.g. Bruno et. al., 2020; Degler et. al., 2018; Heilbron et. al., 2017b; Ávila et. al., 2014; Duarte et. al., 2004) (Figure 19a). For the Mineiro Belt, our interpretation follows the model recently proposed by Araujo et al. (2019a) in which a double-sided subduction was responsible for the origin of magmatic arc plutonic rocks and supracrustal units. For the Juiz de Fora magmatic arc, eastward subduction is necessary to explain the geochemical zoning described by Heilbron et al (2010). Double-sided subduction for the Mineiro Belt also seems necessary to explain the ca. 2.1-2.05 Ga late-to post-collisional granitoids observed in the Piedade block and to account for the dome-and-keel structure that affected the foreland of the São Francisco paleocontinent (eg. Cutts et. al., 2018).

This stage in geologic record (ca. 2.1 – 1.9 Ga) is marked by the generation of high Ba-Sr granitoid rocks in the Mineiro Belt, Mantiqueira and the Juiz de Fora Complexes (Figure 19b) (Bruno et. al., 2020, Araújo et. al., 2019b; Moreira et. al., 2018; Heilbron et al., 2010, Duarte et. al., 2004). The ca. 2.1 Ga accretion of these terranes against the Archean Campo Belo complex took place along a suture zone referred as the Jeceaba-Bom Sucesso lineament (Moreira et. al., 2018, Alkmim & Teixeira, 2017, Ávila et. al., 2010).

The ensuing late- to post-collisional magmatism generated ca. 2.05 Ga high-K granitoid rocks and adakites in the Campo Belo complex (samples 48A and 48B). An important tectono-metamorphic episode has been recognized at ca. 2.05 – 2.04 Ga by Heilbron et al. (2010) and a granulite facies metamorphic event at ca. 2.05 Ga by Bruno et. al. (2020) at the Ponte Nova suture zone. The latter is thought to correspond to the collision

between the Mantiqueira Complex and the Piedade Block, which took place coeval to the development of the Abre Campo suture zone between the Mantiqueira and Juiz de Fora Complexes (Degler et. al., 2018; Heilbron et. al., 2010). This time interval is also marked by the late- to post-collisional magmatism in the Piedade Block with the crystallization of tholeiitic metabasic (Sample 70A) and alkaline rocks (Sample 58A) (Figure 19d), which are diagnostic of extensional intraplate settings, with associated adakites (sample 58B) and biotite-bearing or two-mica granites (Samples 65, 68A, 70B) related to coeval melting of continental crust. Coeval 2.05 Ga post-collisional processes in the foreland zone of this orogenic system are represented by 'dome-and-keel' tectonics in and by the sedimentation of quarzitic sediments of the Itacolomi Group overlying the inverted Minas Supergroup passive margin successions (Cutts et. al., 2018; Machado, et. al., 1996).

The ca. 1.9 Ga orogenic collapse stage in the southern São Francisco Paleocontinent is marked by the presence of within-plate alkaline basalts with OIB-like signatures and of alkaline rocks (Figure 19b) (Bruno et. al., 2020, Cutts, et. al., 2019, Heilbron et. al., 2010).

7.3 Regional Correlations and implications for the assembly of the Columbia supercontinent

The determination of precise ages and isotopic signatures of Archean and Paleoproterozoic tectono-stratigraphic terranes in different cratons is an important tool in understanding the processes that led to the formation of the first supercontinents (Terentiev & Santosh, 2020; D'Agrella-Filho et. al., 2020; Iaccheri & Bargas, 2020; Wu et. al., 2020; D'Agrella-Filho & Cordani, 2017; Meert & Santosh, 2017; Xu et. al., 2014; Condie, 2013; Mitchell et. al., 2012/ Rogers & Santosh 2009). Additional to the contribution made by paleomagnetism, correlations between the periods of major juvenile

622 crustal growth and recycling play an important role in such reconstructions (e.g. Cawood,
623 et. al., 2016; Condie, 2013; Santosh, 2009). Several authors (Evans & Mitchell, 2011;
624 Yakubchuk, 2010; Zhao et. al., 2004) postulate the assembly of the Columbia
625 supercontinent during the ca. 1.9 Ga global peak in accretionary orogenesis but others
626 suggest a later assembly at ca. 1.6 Ga (e.g. Terentiev & Santosh, 2020; Caxito et. al.,
627 2020b; Meert & Santosh, 2017; Pisarevsky et. al., 2014; Rogers & Santosh, 2009).

628 Within the units of the São Francisco Paleocontinent, the ca. 2.4 to 2.07 Paleoproterozoic
629 granitoid rocks with high Ba-Sr, sanukitoid and TTG signatures suggest a complex and
630 diachronous subduction history (Bruno et. al., 2020; Cutts, et. al., 2020; Araújo et. al.,
631 2019b; Moreira, et. al., 2018; Degler et. al., 2018; Heilbron et. al., 2017b; Teixeira et. al.,
632 2015, Seixas et. al., 2013). Late- to post-collisional granitoid rocks between ca. 2.1 and
633 2.06 Ga and an important metamorphic record at ca. 2.05 to 2.04 Ga, with the
634 development of associated foreland basins marked the final transition to extensional
635 collapse (Cutts, et. al., 2019; Alkmim & Teixeira, 2017; Aguilar Gil et. al., 2015; Vlach
636 et. al., 2003; Brueckner et. al., 2000; Machado et. al., 1992).

637 The southern Archean complexes of the São Francisco Paleocontinent (e.g. Bonfim, Belo
638 Horizonte, Santa Bárbara), and the reworked Campo Belo Complex may represent the
639 southern continuation of the Archean Gavião Block (Figure 20a). Minor Archean
640 continental blocks such as the Piedade, Guanhães, Guararema, Jequié and Serrinha were
641 welded together as a result of Paleoproterozoic accretionary tectonics and were intruded
642 by large volumes of plutonic rocks generated by crustal recycling and addition of juvenile
643 arcs. Parts of the Minas-Bahia Orogen display more accretionary characteristics, such as
644 the Mineiro Belt, the Juiz de Fora, and the Buerarema Complex. Others, such as the
645 Itabuna-Salvador-Curaçá Belt and the Mantiqueira Complex, show both juvenile
646 additions within Cordilleran tectonic settings (Figure 20b).

Our proposed tectonic scenario involves the coeval development of passive margins around the Archean blocks and outboard juvenile arcs at ca. 2.6 Ga, followed by a period of arc-related magmatism (with both Cordilleran and intra-oceanic signatures), building the Paleoproterozoic orogenic belt at ca. 2.4 to 2.06 Ga (Figure 20). All the various crustal fragments were diachronously amalgamated between 2.1 and 2.04 Ga, with the development of foreland basins and metamorphic core complexes. The orogenic cycle was terminated by bimodal magmatism and extensional deformation between 2.02 to 1.9 Ga, altogether interpreted as related to slab detachment and orogenic collapse (Bruno et. al., 2020; Cutts, et. al., 2020; Araújo et. al., 2019b; Cutts et. al., 2019; Moreira, et. al., 2018; Degler et. al., 2018; Alkmim & Teixeira, et. al., 2017; Heilbron et. al., 2017b; Teixeira et. al., 2017a; Teixeira et. al., 2015, Aguilar Gil et. al., 2015; Seixas et. al., 2013; Vlach et. al., 2003; Brueckner et. al., 2000; Machado et. al., 1992).

The assembly of the São Francisco Paleocontinent by the amalgamation of Archean blocks and Rhyacian orogens before ca. 2.0 Ga is similar in its timing and mechanism to the formation of the West Africa Block/Central African Block/Transamazonian (Terentiev & Santosh, 2020; Caxito et. al., 2020a; D'Agrella-Filho et. al., 2017; Cordani et al., 2013), both prior to the main orogenic period that consolidated the Columbia supercontinent (Figure 21a). Similar accretionary processes had terminated by ca. 1.95 Ga in the Khondalite Belt of North China (Li et. al., 2020; Liu et al., 2012; Santosh, 2010). However, based on paleomagnetic poles in mafic dykes (ca. 1.7 Ga), that crop out in most of the building blocks of Columbia, and the geometry of Paleoproterozoic belts, D'Agrella-Filho et. al., (2020) proposed that the Rio de la Plata, São Francisco-Congo, North China, and India blocks were all connected as part of Columbia by this time (Figure 21b). Zhao et. al. (2004) suggests the proximity of the São-Francisco Congo and the North

China cratons due to Statherian dyke swarms and related volcanic rocks, supported by paleomagnetic poles (Xu et. al., 2020; Salminen et. al., 2016).

8. Concluding Remarks

The reworked basement units of the external segments of the Neoproterozoic Brasília and Ribeira Orogenic Belts, SE Brazil, are considered to be part of the Minas-Bahia Orogenic Belt, despite the Brasiliano metamorphic overprint (ca. 600-560 Ma). Integrating new data with previous contributions a protracted orogenic cycle, from subduction to collisional stages and a subsequent orogenic collapse with associated magmatism. Cordilleran magmatic arcs that developed along the margins of Archean microcontinents (e.g. Mantiqueira Complex) and intra-oceanic juvenile accretionary arcs (e.g. Mineiro Belt and Juiz de Fora Complex) were diachronously amalgamated with Archean nuclei to form the São Francisco-Congo Paleocontinent, between 2.1 to 2.05 Ga. The collisional episodes were followed by tectonic collapse, associated with bimodal magmatism between 2.05 and 1.98 Ma. The presence of Archean and Paleoproterozoic TTG, sanukitoids and adakitic rocks point to the importance of subduction processes as driving forces building the São Francisco-Congo Paleocontinent.

Finally, our contribution to unravelling the Minas-Bahia Orogenic Belt, in the context of supercontinent cycles, suggests that a large continental landmass was amalgamated during the Rhyacian (ca. 2.1-2.05 Ga). Together with Baltica, Amazonia and West Africa, the São-Francisco Congo is surrounded by a broad Paleoproterozoic (pre-Columbia) oceanic realm. After the orogeny, Orosirian bimodal magmatic successions point to an extensional tectonic setting, hampering any direct connections with Columbia before ca. 1.9 Ga.

Acknowledgments

The authors thank the facilities and the help from all the technical support of the laboratories (LGPA, LAGIR) of the Geology Institute at UERJ, the Rio de Janeiro State University. We would also like to thank our partners from universities in Brazil (USP, UNB, UFOP) and abroad (UQAM and Edmonton, Canada; Portsmouth, UK; Notre Dame, US; ANU, Australia, Salzburg, Austria) for the analytical data during the last 30 years. We thank Prof. M. Santosh, Dr. Andrea Festa and two anonymous reviewers for all the contributions that helped improve the manuscript. We should thank FAPERJ and funding agencies, and joint projects with CPRM and Petrobras. This is contribution to IGCP 648.

References

Aguilar, C., Alkmim, F.F., Lana, C.C., Farina, F. 2017. Paleoproterozoic assembly of the São Francisco craton, SE Brazil: new insights from U–Pb titanite and monazite dating. Precambrian Research. 289, 95-115.

Aguilar Gil, C., Farina, F., Lana, C., 2015. Constraining the timing of the Transamazonian metamorphic event in the Southern São Francisco Craton (Brazil): revealed by monazite and titanite dating. 8th Hutton Symposium on Granites and Related Rocks, Florianópolis, Brazil.

Albert, C., Farina, F., Lana, C., Stevens, G., Storey, C., Gerdes, A., Dopico, C. 2016. Archean crustal evolution in the Southern São Francisco craton, Brazil: Constraints from U-Pb, Lu-Hf and O isotope analyses. Lithos 266-267, 64-86.

Alkmim, F.F. & Teixeira, W., 2017. The Paleoproterozoic Mineiro belt and the Quadrilátero Ferrífero. In: Heilbron M., Alkmim F., Cordani U.G. (Guest Ed.), The São Francisco Craton and its margins, Eastern Brazil. Regional Geology Review Series. Springer-Verlag, Chapter 5, 71–94.

Alkmim, F.F. Kuchenbecker, M. Reis, H. L.S., Pedrosa-Soares, A.C. 2017. The Araçuaí Belt. In: Heilbron M., Alkmim F., Cordani U.G. (Guest Ed.), The São Francisco Craton and its margins, Eastern Brazil. Regional Geology Review Series. Springer-Verlag, Chapter 14, 255–276.

Alkmim F.F., Marshak S., Pedrosa-Soares A.C., Peres G.G., Cruz S.C.P., Whittington A. 2006. Kinematic evolution of the Araçuaí-West Congo orogeny in Brazil and Africa: Nutcracker tectonics during the Neoproterozoic assembly of Gondwana. Precambrian Research. 149, 43–64.

Alkmim FF, Noce CM. 2006. Outline of the geology of Quadrilátero Ferrífero. In: Alkmim FF, Noce CM (eds) The Paleoproterozoic Record of São Francisco Craton. IGCP 509 Field Workshop, Bahia and Minas Gerais. Field Guide and Abstracts, 37–73.

Almeida, F.F.M.1981. O Cráton do Paramirim e suas relações com o do São Francisco. In: Simpósio Sobre o Cráton do São Francisco e Suas Faixas Marginais. Salvador. 1–10.

Araújo, A.J.D., Bongiolo, E.M., Ávila, C.A. 2019a. The southern São Francisco Craton puzzle: Insights from aerogeophysical and geological data. Journal of South American Earth Sciences 94, 10203.

Araújo, L.E.A.B., Heilbron, M., Valeriano, C.M., Teixeira, W., Neto, C.C.A. 2019b. Lithogeochemical and Nd-Sr isotope data of the orthogranulites of the Juiz de Fora complex, SE-Brazil: insights from a hidden Rhyacian Orogen within the Ribeira belt. Brazilian Journal of Geology 49, 3.

Atherton M., Petford N. 1993. Generation of sodium-rich magmas from newly underplated basaltic crust. Nature 362, 144–146.

754 Ávila, C.A., Teixeira, W., Bongiolo, E.M., Dussin, I.A., 2014. The Tiradentes suite and
755 its role in the Rhyacian evolution of the Mineiro belt, São Francisco Craton: Geochemical
756 and U-Pb geochronological evidence. Precambrian Research. 243, 221–251.

757 Ávila, C.A., Teixeira, W., Cordani, U.G., Moura, C.A.V., Pereira, R.M..2010. Rhyacian
758 (2.23–2.20 Ga) juvenile accretion in the southern São Francisco Craton, Brazil:
759 geochemical and isotopic evidence from the Serrinha magmatic suite, Mineiro Belt.
760 Journal of South American Earth Sciences. 29, 464-484.

761 Barbosa, N.S., Teixeira W., Ávila C.A., Montecinos P.M., Bongiolo E.M. 2015. 2.17–
762 2.10 Ga plutonic episodes in the Mineiro belt, São Francisco Craton, Brazil: U-Pb ages,
763 geochemical constraints and tectonics Precambrian Research. 270, 204-225

764 Barbosa, J.S.F. & Barbosa, R.G., 2017. The Paleoproterozoic Eastern Bahia Orogenic
765 Domain. In: Heilbron M., Alkmim F., Cordani U.G. (Guest Ed.), The São Francisco
766 Craton and its margins, Eastern Brazil. Regional Geology Review Series. Springer-
767 Verlag, Chapter 4, 57-70.

768 Barbosa, J.S.F., Sabaté, P., 2004. Archean and Paleoproterozoic crust of the São
769 Francisco Craton, Bahia, Brazil: geodynamic features. Precambrian Research, 133, 1–27.

770 Bersan, S.M., Costa, A.F.O., Danderfer, A., Abreu, F.R., Lana, C., Queiroga, G., Storey,
771 C. Moreira, H. 2020. Paleoproterozoic juvenile magmatism within the northeastern sector
772 of the São Francisco paleocontinent: Insights from the shoshonitic high Ba–Sr
773 Montezuma granitoids. Geoscience Frontiers. 11 (5)., 1821-1840.

774 Bersan, S.M., Danderfer Filho A., Abreu F. R., Lana, C. 2018. Petrography, geochemistry
775 and geochronology of the potassic granitoids of the Rio Itacambiruçu Supersuite:
776 implications for the Meso- to Neoarchean evolution of the Itacambira-Monte Azul block.
777 Brazilian Journal of Geology. 48(1), 1-24.

778 Boynton, W.V. 1984. Cosmochemistry of the rare earth elements: meteorite studies In:
779 P. Henderson (Ed.), Rare Earth Element Geochemistry. Developments in Geochemistry.
780 2, 63-114

781 Brito-Neves, B.B., 2002. Main stages of development of sedimentary basins of South
782 America and their relationships of tectonics of supercontinents. Gondwana Research. 5,
783 175–196.

784 Brito-Neves, B.B., Campos Neto M.C., Fuck R., 1999. From Rodinia to Western
785 Gondwana: An approach to the Brasiliano/Pan-African cycle and orogenic collage.
786 Episodes. 22, 155–199.

787 Brueckner, H.K., Cunningham, D., Alkmin, F.F., Marshak, S., 2000. Tectonic
788 implications of Precambrian Sm–Nd dates from the southern São Francisco craton and
789 adjacent Araçuai and Ribeira belts, Brazil. Precambrian Research. 99 (3), 255–269.

790 Bruno H., Elizeu V., Heilbron M., Valeriano C.M., Strachan R., Fowler M., Bersan S.,
791 Moreira H., Dussin I., Silva L.G.E.S., Tupinambá M., Almeida J., Dunlop J., Neto C.,
792 Carvalho M., Almeida R., Storey C. 2020. Neoarchean and Rhyacian TTG-Sanukitoid

suites in the southern São Francisco Paleocontinent, Brazil: Evidence for diachronous change towards modern tectonics. Geoscience Frontiers 11 (5), 1763-1787.

Bucholz C. E., Stolper E. M., Eiler J.M., Breaks F. W. 2018. A Comparison of Oxygen Fugacities of Strongly Peraluminous Granites across the Archean–Proterozoic Boundary. Journal of Petrology 59 (11), 2123–2156.

Campos Neto, M.C. 2000. Orogenic Systems from Southwestern Gondwana: An approach to Brasiliano-Pan African Cycle and Orogenic Collage in Southeastern Brazil. In: Cordani, U.G.; Milani, E.J.; Thomaz Filho, A.; Campos, D.A. (eds.) Tectonic Evolution of South América. Rio de Janeiro, 31st International Geological Congress, Rio de Janeiro, 335–365.

Cardoso, C.D., Ávila, C.A., Neumann, R. Oliveira, E.P., Valeriano, C.M., Dussin, I.A. 2019. A Rhyacian continental arc during the evolution of the Mineiro belt, Brazil: Constraints from the Rio Grande and Brumado metadiorites. Lithos 326-327, 246-264.

Caro, G. & Bourdon, B. 2010. Non-chondritic Sm/Nd ratio in the terrestrial planets: Consequences for the geochemical evolution of the mantle–crust system. Geochimica et Cosmochimica Acta. 74(11), 3333-3349.

Castillo P.R., Janney P.E., Solidum R. 1999. Petrology and geochemistry of CamiguinIsland, southern Philippines: insights into the source of adakite and other lavasin a complex arc tectonic setting. Contributions to Mineralogy and Petrology 134, 33–51

Castillo P.R. 2012. Adakite petrogenesis. Lithos 134-135, 304-316.

Cawood, P.A., Strachan, R.A., Pisarevsky, S.A., Gladkochub, D.P., Murphy, J.B. 2016. Linking collisional and accretionary orogens during Rodinia assembly and breakup: implications for models of supercontinent cycles. Earth Planetary Science Letters 449, 118-126.

Cawood, P.A. & Buchan, C. 2007. Linking accretionary orogenesis with supercontinent assembly. Earth-Science Reviews 82, 217-256.

Caxito, F., Santos, L.M.C.L., Ganade, C.E., Bendaoud, A., Fettous, E.H., BouyoHouketchang, M. 2020a. Toward an integrated model of geological evolution for NE Brazil–NW Africa: the Borborema Province and its connections to the Trans-Saharan (Benino-Nigerian and Tuareg shields) and Central African orogens. Brazilian Journal of Geology. 50, e20190122.

Caxito, F., Hagemann, S., Dias, T. G., Barrote, V., Dantas, E.L., Chaves, A.O., Campello, M. S., Campos, D.C. 2020b. A magmatic barcode for the São Francisco Craton: Contextual in-situ SHRIMP UPb baddeleyite and zircon dating of the Lavras, Pará de Minas and Formiga dyke swarms and implications for Columbia and Rodinia reconstructions. Lithos.374-375, 105708.

Caxito, F., Uhlein, Al., Dantas, E., Stevenson, R., Egydio-Silva, M., Salgado, S. The Ripo Preto and Riacho do Pontal Belts. 2017. In: Heilbron M., Alkmim F., Cordani U.G. (Guest

Ed.), The São Francisco Craton and its margins, Eastern Brazil. Regional Geology Review Series. Springer-Verlag, Chapter 12, 221–239.

Chung, S.L., Liu, D.Y., Ji, J.Q., Chu, M.F., Lee, H.Y., Wen, D.J., Lo, C.H., Lee, T.Y., Qian, Q., Zhang, Q., 2003. Adakites from continental collision zones: melting of thickened lower crust beneath southern Tibet. Geology 31, 1021–1024.

Collins, A.S. & Pisarevsky S.A. 2005. Amalgamating eastern Gondwana: the evolution of the Circum-Indian Orogens. Earth-Science Reviews 71, 229-270.

Condie, K.C. 2013. Preservation and recycling of Crust during accretionary and collisional phases of Proterozoic Orogens: a bumpy road from Nuna to Rodinia. Geosciences 3,240-261.

Condie, K.C. 2011. The supercontinent cycle Earth as an Evolving Planetary System, Academic Press, 317-355.

Cordani, U.G., Pimentel, M.M., Ganade de Araújo, C.E.G., Fuck, R.A., 2013. The significance of the Transbrasiliano-Kandy tectonic corridor for the amalgamation of West Gondwana. Brazilian Journal of Geology 43, 583–597.

Cordani, U.G. and Sato, K. 1999. Crustal evolution of the South American Platform based on Sm-Nd isotopic systematic on granitoid rocks. Episodes. 22, 167–173.

Corrêa Neto AV, Modesto AM, Caputo Neto V, Guerrero JC. 2012. Alteração hidrotermal em zona de cisalhamento associada ao Lineamento Congonhas, sul do Quadrilátero Ferrífero, Minas Gerais. Anuario Instituo Geociências 35 (2), 55–64.

Costa A.F.O., Danderfer A., Bersan S.M. 2017. Record of a Statherian rift-sag basin in the Central Espinhaço Range: Facies characterization and geochronology. Journal of South American Earth Sciences 82, 311-328.

Cox, K.G, Bell, J.D., Pankhurst. 1979. The Interpretation of Igneous Rocks. Allen &Unwin, London.

Cruz, S.C.P., Barbosa, J.S.F., Pinto, M.S., Peucat, J.-J., Paquette, J.L., Santos de Souza, J., de Souza Martins, V., Chemale Jr, F.., Carneiro, M.A. 2016. The Siderian-Orosirian magmatism in the Archean Gavião Paleoplate, Brazil: U–Pb geochronology, geochemistry and tectonic implications. Journal of South American Earth Sciences. 69, 43-79.

Cutts, K., Lana, C., Moreira, H., Alkmim, F. Peres, G. 2020. Zircon U-Pb and Lu-Hf record from high-grade complexes within the Mantiqueira Complex: First evidence of juvenile crustal input at 2.4–2.2 Ga and implications for the Palaeoproterozoic evolution of the São Francisco Craton. Precambrian Research 338, 105567.

Cutts, K., Lana, C., Alkmim, F., Farina, F., Moreira, H., Coelho, V. 2019. Metamorphism and exhumation of basement gneiss domes in the Quadrilátero Ferrífero: Two stage dome-and-keel evolution? Geoscience Frontiers 10 (5), 1765-1787.

869 D'Agrella-Filho, M.S., Teixeira, W., Trindade, R.I.F., Patroni, O.A.L., Prieto, R.F. 2020.
870 Paleomagnetism of 1.79 Ga Pará de Minas maficdykes: Testing a São Francisco/Congo-
871 North China-Rio de la Plata connection in Columbia. Precambrian Research 338, 105584.

872 D'Agrella-Filho, M.S. & Cordani, U.G. 2017. The Paleomagnetic Record of the São
873 Francisco-Congo Craton. In: Heilbron M., Alkmim F., Cordani U.G. (Guest Ed.), The
874 São Francisco Craton and its margins, Eastern Brazil. Regional Geology Review Series.
875 Springer-Verlag, Chapter 17, 321–331.

876 Danderfer A., Lana C.C., Nalini Júnior H.A., Costa A.F.O. 2015. Constraints on the
877 Statherian evolution of the intraplate rifting in a Paleo-Mesoproterozoic paleocontinent:
878 New stratigraphic and geochronology record from the eastern São Francisco craton.
879 Gondwana Research 28(2), 668-688.

880 De Paolo, D.J. 1981. Trace Element and Isotopic Effects of Combined Wallrock
881 Assimilation and Fractional Crystallization. Earth and Planetary Science Letters, 53, 189-
882 202.

883 Degler, R., Pedrosa-Soares, A. C., Novo, T., Tedeschi, M. Silva, l.C., Dussin, I., Lana, C.
884 2018. Rhyacian-Orosirian isotopic records from the basement of the Araçuaí-Ribeira
885 orogenic system (SE Brazil): Links in the Congo-São Francisco palaeocontinent.
886 Precambrian research. 317, 179-195.

887 Drummond, M.S., Defants, M.J., 1990. A model for Trondhjemite-Tonalite-Dacite
888 genesis and crustal growth via slab melting: archean to modern comparisons. Journal of
889 Geophysical Research 95, 21503–21521

890 Duarte, B.P., Valente, S.C., Heilbron, M., Campos Neto, M.C. 2004. Petrogenesis of the
891 orthogneisses of Mantiqueira Complex, central Ribeira belt, SE Brazil: An Archaean to
892 Palaeoproterozoic basement unit reworked during the Pan-African Orogeny. Gondwana
893 Research. 7 (2), 437–450.

894 Evans D.A.D., Mitchell R.N. 2011. Assembly and breakup of the core of
895 paleoproterozoic-mesoproterozoic supercontinent Nuna Geology, 39, 443-446

896 Farina F, Albert C, Lana C. 2015. The Neoarchean transition between medium- and high-
897 K granitoids: Clues from the Southern São Francisco Craton (Brazil). Precambrian
898 Research 266, 375–394.

899 Frost, B.R., Barnes, C.G., Collins, W.J., Arculus, R.J., Ellis, D.J, Frost, C.D. 2001. A
900 geochemical classification for granitic rocks. Journal of Petrology. 42, 2033-2048.

901 Gao, S., Rudnick, R.L., Yuan, H.L., Liu, X.M., Liu, Y.S., Xu, W.L., Lin, W.L., Ayerss,
902 J., Wang,X.C., Wang, Q.H. 2004. Recycling lower continental crust in the North China
903 craton. Nature 432, 892–897

904 Goulart, L.E.A., Carneiro M.A., Endo I., Suita M.T.F. 2013. New evidence of
905 Neoarchean crustal growth in southern São Francisco Craton: the Carmópolis de Minas
906 Layered Suite, Minas Gerais, Brazil. Brazilian Journal of Geology. 43(3). 445–459

907 Halla, J., van Hunen, J., Heilimo, E., Hölttä, P., 2009. Geochemical and numerical
908 constraints on Neoarchaean plate tectonics. Precambrian Research 174, 155–162.

Hartmann L.A., Endo I., Suita M.T.F., Santos J.O.S., Frantz J.C., Carneiro M.A., Naughton N.J., Barley M.E., 2006. Provenance and age delimitation of Quadrilátero Ferrífero sandstones based on zircon U–Pb isotopes. Journal of South American Earth Sciences, 20, 273–285.

Hawkesworth, C.J., Dhuime, B., Pietranik, A.B., Cawood, P.A., Kemp, A.I.S., Storey, C.D. 2010. The generation and evolution of the continental crust. Journal of the Geological Society of London 167, 229-248.

Heilbron, M., Cordani, U.G., Alkmim, F.F. 2017a. The São Francisco Craton and its margins. In: Heilbron M., Alkmim F., Cordani U.G. (Guest Ed.), The São Francisco Craton and its margins, Eastern Brazil. Regional Geology Review Series. Springer-Verlag, Chapter 1, 3-14.

Heilbron, M., Ribeiro, A., Valeriano, C.M., Paciullo, F.V., Almeida, J.C.H., Trouw, R.J.A., Tupinambá, M. Eirado, L.G. 2017b. The Ribeira Belt. In: Heilbron M., Alkmim F., Cordani U.G. (Guest Ed.), The São Francisco Craton and its margins, Eastern Brazil. Regional Geology Review Series. Springer-Verlag, Chapter 15, 277-302.

Heilbron, M, Duarte B.P., Valeriano C.M., Simonetti A, Machado N, Nogueira, J.R. .2010. Evolution of reworked Paleoproterozoic basement rocks within the Ribeira belt (Neoproterozoic), SE-Brazil, based on U-Pb geochronology: Implications for paleogeographic reconstructions of the São Francisco-Congo paleocontinent. Precambrian Research. 178, 136–148

Heilimo, E., Halla, J., Hölttä, P. 2010. Discrimination and origin of the sanukitoid series: Geochemical constraints from the Neoarchean western Karelian Province (Finland). Lithos 115, 27-39.

Heron, P.J., Lowman, J.P., Stein, C. 2015. Influences on the positioning of mantle plumes following supercontinent formation. Journal of Geophysics Research, Solid Earth 120, 3628-3648.

Huang X.I., Xu Y.G., Lan J.B., Yang.J., Luo Z.Y. 2009. Neoproterozoic adakitic rocks from Mopanshan in the western Yangtze Craton: partial melts of a thickened lower crust. Lithos 112, 367-381.

Iaccheri, L.M & Bargas, L. 2020. Zircon provenances provide paleogeographic constraints on models reconstructing the Paleoproterozoic Columbia Supercontinent. Gondwana Research 82, 254 – 266.

Irvine, T.M. & Baragar, W.R. 1971. A guide to the chemical classification of common volcanic rocks. Canadian Journal of Earth Sciences. 8, 523-548.

Kay, R.W., Kay, S.M., 2002. Andean adakites: three ways to make them. Acta PetrologicaSinica 18, 303–311.

Kuribara, Y., Tsunogae, T., Santosh, M., Takamura, Y., Costa, A.G., Rosière, C.A. 2019. Eoarchean to Neoproterozoic crustal evolution of the Mantiqueira and the Juiz de Fora Complexes, SE Brazil: Petrology, geochemistry, zircon U-Pb geochronology and Lu-Hf isotopes. Precambrian Research. 323, 82-101.

Lana, C., Alkmim, F.F., Armstrong, R., Scholz, R., Romano, R., Nalini Jr., H.A. 2013. The ancestry and magmatic evolution of Archaean TTG rocks of the Quadrilátero Ferrífero province, southeast Brazil. Precambrian Research. 231, 157–173.

Laurent, O., Auwera, J.V., Bingen, B., Bolle, O., Gerdes, A. 2019. Building up the first continents: Mesoarchean to Paleoproterozoic crustal evolution in West Troms, Norway, inferred from granitoid petrology, geochemistry, and zircon U-Pb/Lu-Hf isotopes. Precambrian Research 321, 303-327.

Laurent, O., Martin H., Moyen J.F., Doucelance R. 2014. The diversity and evolution of late Archean granitoids: evidence for the onset of 'modern-style' plate tectonics between 3.0 and 2.5 Ga. Lithos 205, 208–235.

Laurent, O., Martin, H., Doucelance, R., Moyen, J.-F., Paquette, J.-L., 2011. Geochemistry and petrogenesis of high-K "sanukitoids" from the Bulai pluton, Central Limpopo Belt, South Africa: implications for geodynamic changes at the Archean–Proterozoic boundary. Lithos 123, 73–91.

Li, C., Li, L., Li, SR, Santosh, M. 2020. Late Paleoproterozoic mafic-intermediate dykes from the southern margin of the North China Craton: Implication for magma source and Columbia reconstruction. Precambrian Research. 347, 105837.

Liu J., Zhang K., Yin C., Cheng C., Liu X., Zhao C., Chen Y., Wang X. 2020. Synchronous A-type and adakitic granitic magmatism atca.2.2 Ga in the Jiao–Liao–Ji belt, North China Craton: Implications for rifting triggered by lithospheric delamination. Precambrian Research 342, 105629.

Liu S.-W., Zhang J., Li Q.-G., Zhang L.F., Wang W., Yang P.T. 2012. Geochemistry and U-Pb zircon ages of metamorphic volcanic rocks of the Paleoproterozoic Lvliang Complex and constraints on the evolution of the Trans-North China Orogen, North China Craton. Precambrian Research., 222–223, 173-190.

Lowman J.P. & Jarvis, G.T. 1995. Mantle convection models of continental collision and breakup incorporating finite thickness plates. Phys. Earth Planet. Inter. 88, 53-68.

Machado, N., Schrank, A., Noce, C.M., Gauthier, G. 1996. Ages of detrital zircon from Archean-Paleoproterozoic sequences: Implications for Greenstone Belt setting ans evolution of a Transamazonian foreland basin in Quadrilátero Ferrífero, southeast Brazil. Earth and Planetary Science Letters, 141, 259–276.

Machado, N. & Carneiro, M.A. 1992. U − Pb evidence of late Archean tectono-thermal activity in the southern São Francisco shield, Brazil. Canadian Journal of Earth Sciences. 29, 2341–2346.

Martin H., Moyen, J.F., Rapp R. 2010. Sanukitoids and the Archean-Proterozoic boundary. Transactions of the Royal Society of Edinburgh 100, 15-33.

Martin H., Smithies R.H., Rapp R.P., Moyen J.-F., Champion D.C. 2005. An overview of adakite, tonalite–trondhjemite–granodiorite (TTG) and sanukitoid: relationships and some implications for crustal evolution. Lithos, 79, 1–24.

McDonough, W.F. & Sun, W. The composition of the Earth. 1995. Chemical Geology. 120 (3-4), 223-253.

Meert, J.G. & Santosh, M. 2017. The Columbia supercontinent revisited. Gondwana Research 50, 67-83.

Meschede M. 1986. A method of discriminating between different types of midocean ridge basalts and continental tholeiites with the Nb–Zr–Y diagram Chem. Geol. 56, 207-218.

Mitchel, R.N., Kylian, T.M., Evans D.A.D., 2012. Supercontinent cycles and the calculation of absolute palaeolongitude in deep time. Nature 482, 208-211.

Moreira H., Seixas L., Storey C., Fowler M., Lasalle S., Stevenson R., Lana C. 2018. Evolution of Siderian juvenile crust to Rhyacian high Ba-Sr magmatism in the Mineiro Belt, southern São Francisco Craton. Geoscience Frontiers 4, 977-995.

Moyen, J.-F. 2019. Archean granitoids: classification, petrology, geochemistry and origin. Geologica l Society, London, Special Publications, SP489-2018–34.

Moyen, J.F. & Laurent, O. 2018. Archaean tectonic systems: A view from igneous rocks. Lithos 302-303, 99-125.

Moyen, J.F., Martin, H., 2012. Forty years of TTG research. Lithos 148, 312–336.

Murphy, J.B., Nance, R.D. 2012. Speculations on the mechanisms for the formation and breakup of supercontinents. Geoscience Frontiers 4, 185-194.

Næraa, T., Scherstén, A., Rosing, M.T., Kemp, A.I.S., Hoffmann, J.E., Kokfelt, T.F., Whitehouse, M.J. 2012. Hafnium isotope evidence for a transition in the dynamics of continental growth 3.2 Gyr ago. Nature Research Letter, 485. 627 – 631.

Nance, R.D. 2019. The supercontinent cycles. Reference Module in Earth Systems and Environmental Sciences.

Noce, C.M., Pedrosa-Soares, A.C., Silva, L.C., Armstrong, R., Piuzana, D. 2007. Evolution of polycyclic basement in the Araçuaí Orogen based on U-Pb SHRIMP data: implications for the Brazil-Africa links in the Paleoproterozoic time. Precambrian Research. 159, 60–78.

Noce C.M., Teixeira W., Quéméneur J.J.G., Martins V.T.S. Bolzachini E. 2000. Isotopic signatures of Paleoproterozoic granitoids from southern São Francisco Craton, NE Brazil, and implications for the evolution of the Transamazonian Orogeny. Journal of South American Earth Sciences, 13, 225–239.

PatiñoDouce A.E.P. 1999. What do experiments tell us about the relative contributions of crust and mantle to the origin of granitic magmas? Geological Society, London, Special Publications 168, 55-75.

Pearce, J.A. 1982. Trace element characteristics of lavas from destructive plate boundaries. In: R S Thorpe (ed) Andesites: Orogenic Andesites and Related Rocks. John Wiley & Sons, Chichester, pp 525-548, ISBN 0 471 28034 8

Peccerillo, A. & Taylor, S.R. 1976. Geochemistry of Eocene calc-alkaline volcanic rocks from the Kastamonu area, Northern Turkey. Contribution to Mineralogy and Petrology. 58, 63-81.

Pedrosa Soares, A.C.; Noce, C.M.; Wiedemann, C.M.; Pinto, C. P. 2001. The Araçuaí-West-Congo Orogen in Brazil: an overview of a confined orogen formed during Gondwanaland assembly. Precambrian Research 110(1–4), 307–323.

Peres, G.G., Alkmim, F.F., Jordt-Evangelista, H. 2004. The southern Araçuaí belt and the Dom Silvério Group: Geologic architecture and tectonic significance. Anais da Academia Brasileira de Ciências. 76, 771–790.

Pinheiro, M.A.P., Suita, M.T.F., Lesnov, F.P., Tedeschi, M., Silva, L.C., Medvedev N.S., Korolyuk V.N., Pinto, C.P., Sergeev, S.A. 2019. Timing and petrogenesis of metamafic-ultramafic rocks in the Southern Brasília orogen: Insights for a Rhyacian multi-system suprasubduction zone in the São Francisco paleocontinent (SE-Brazil) Precambrian Research 321, 328-348.

Pisarevsky S.A., Elming S.-A., Pesonen L.J., Li Z.-X. 2014. Mesoproterozoic paleogeography: Supercontinent and beyond Precambr. Res., 244, 207-225.

Quéméneur, J.J.G., Ribeiro, A., Paciullo, F.V.P., Heilbron, M., Trouw, R.A.J., Valença, J.G., Noce, C.M. 2003. Geologia da Folha Lavras A.C. Pedrosa-Soares, C.M. Noce, R.A.J. Trouw, M. Heilbron, orgs (Eds.), Geologia e Recuros Minerais do Sudeste Mineiro, vol. 1, Projeto Sul de Minas, 259-319.

Rajesh, H.M., Belyanin, G.A., Van Reenen, D.D. 2018. Three tier transition of Neoarchean TTG-sanukitoid magmatism in the Beit Bridge Complex, Southern Africa. Lithos 296-299, 431-451.

Reis, H.LS., Alkmim, F.F., Fonseca, R.C.S., Nascimento, T.C., Suss, J.F., Prevatti, L. 2017. The São Francisco Basin. In: Heilbron M., Alkmim F., Cordani U.G. (Guest Ed.), The São Francisco Craton and its margins, Eastern Brazil. Regional Geology Review Series. Springer-Verlag, Chapter 7, 117–143.

Rogers, J. & Santosh, M. 2009. Tectonics and surface effects of the supercontinent Columbia. Gondwana Research. 15 (3-4), 373-380.

Rogers, J.J.W. & Santosh, M. 2002. Configuration of Columbia, a Mesoproterozoic Supercontinent. Gondwana Research 5, 5-22

Romano, R,, Lana, C,, Alkmim, F.F,, Stevens, G,, Armstrong R. 2013. Stabilization of the Southern São Francisco Craton, SE Brazil, through a long-lived and episodic period of potassic magmatism. Precambrian Research, 224, 1–20.

Rooney, T. O., Franceschi, P. & Hall, C. M. 2011. Water-saturated magmas in the Panama Canal region: a precursor to adakite-like magma generation? Contributions to Mineralogy and Petrology 161, 373–388.

Salminen J.M., Evans D.A.D., Trindade R.I.F., Oliveira E.P., Piispa E.J., Smirnov A.V. 2016. Paleogeography of the Congo/São Francisco craton at 1.5 Ga: expanding the core of Nuna supercontinent. Precambrian Res., 286, 195-212.

Santosh, M. 2010.Assembling North China Craton within the Columbia supercontinent: the role of double-sided subduction. Precambrian Research. 178, 149-167.

Santosh, M. & Zhao, G. 2009. (Eds.), Supercontinent Dynamics. Gondwana Research, 15, 225-470.

Seixas, L. A. R., Bardintzeff, J. M., Stevenson, R., Bonin, B., 2013. Petrology of the high-Mg tonalites and dioritic enclaves of the ca. 2130 Ma Alto Maranhão suite: Evidence for a major juvenile crustal addition event during the Rhyacian orogenesis, Mineiro Belt, southeast Brazil. Precambrian Research, 238, 18–41.

Seixas LAR, David J, Stevenson R (2012) Geochemistry, Nd isotopes and U–Pb geochronology of a 2350 Ma TTG suite, Minas Gerais, Brazil: Implications for the crustal evolution of the southern São Francisco craton. Precam Res 196–197, 61–80.

Shand, S. J. 1943. Eruptive rocks, 2nd ed. John Wiley, New York, pp 1-444

Silva, L.C., Pedrosa-Soares, A.C., Armstrong. R., Pinto, C.P., Magalhães, J.T.R., Pinheiro, M.A.P., Santos, G.G. 2016. Disclosing the Paleoarchean to Ediacaran history of the São Francisco craton basement: The Porteirinha domain (northern Araçuaí orogen, Brazil). Journal of South American Earth Sciences. 68, 50-67.

Silva L.C., Armstrong R., Noce C.M., Carneiro M.A., Pimentel M. M., Pedrosa-Soares A.C., Leite C.A., Vieira V.S., Silva M.A., Paes V.J.C., Cardoso-Filho J.M. 2002. Reavaliação da evolução geológica em terrenos pré-cambrianos brasileiros com base em novos dados U-Pb SHRIMP, parte II: Orógeno Araçuaí, Cinturão Mineiro e Cráton São Francisco Meridional. Revista Brasileira de Geociências. 32, 513–528.

Sun, G., Liu, s., Wang, M., Bao, H., Teng, G. 2020. Complex Neoarchean mantle metasomatism: Evidence from sanukitoid diorite-monzodiorite-granodiorite in the northeastern North China Craton. Precambrian Research 342, 105692.

Sun, W. & McDonough, W.F. Chemichal and isotopic systematics of oceanic basalts: Implications for mantle composition and processes. 1989. Geological Society of London Special Publications. 42 (1).

Teixeira, W., Oliveira, E.P., Marques, L.S. 2017a. Nature and Evolution of the Archean Crust of the São Francisco Craton. In: Heilbron M., Alkmim F., Cordani U.G. (Guest Ed.), The São Francisco Craton and its margins, Eastern Brazil. Regional Geology Review Series. Springer-Verlag, Chapter 3, 29-56.

Teixeira, W. Oliveira, E., Peng, P., Dantas, E.L., Hollanda, M.H.B.M. 2017b. U-Pb geochronology of the 2.0 Ga Itapecerica graphite-rich supracrustal succession in the São

Francisco Craton: Tectonic matches with the North China Craton and paleogeographic inferences. Precambrian Research 293, 91-111.

Teixeira, W., Ávila, C.A., Dussin, I.A., Neto, A.C., Bongiolo, E.M., Santos, J.O., Barbosa, N.S., 2015. A juvenile accretion episode (2.35–2.32 Ga) in the Mineiro belt and its role to the Minas accretionary orogeny: Zircon U–Pb–Hf and geochemical evidences. Precambrian Research. 256, 148–169.

Teixeira, W.; Ávila, C.A.; Dussin, I.A.; Vasques, F.S.G.; Hollanda, M. H.M., 2012. Geocronologia U-Pb (LA-ICPMS) em zircão detrítico de rochas metassedimentares paleoproterozoicas da parte sul do Craton do São Francisco: proveniência, delimitação temporal e implicações tectônicas. 12o Simpósio de Geologia do Sudeste/16º Simpósio de Geologia de MG. Nova Friburgo, Sociedade Brasileira de Geologia, Anais, p. 12.

Teixeira, W., Ávila, C.A., Nunes, L.C., 2008. Nd–Sr isotopic geochemistry and U–Pb geochronology of Fé granitic gneiss and Lajedo granodiorite: implications for Paleoproterozoic evolution of the Mineiro belt, southern São Francisco Craton. Geologia USP Série Científica 8, 53–73.

Teixeira, W., Sabaté, P., Barbosa J., Noce, C.M., Carneiro, M.A. 2000. Archean and Paleoproterozoic tectonic evolution of the São Francisco Craton. In: Cordani, U.G.;Milani, E.J.; ThomazFo, A.;Campos, D.A. (eds.) Tectonic Evolution of South América. Rio de Janeiro, 31st International Geological Congress, Rio de Janeiro. 101–137.

Teixeira, W., Carneiro, M.A, Noce C.M, Machado, N., Sato, K., Taylor, P.N. 1996. Pb, Sr and Nd isotopic constraints on the Archean evolution of gneissic-granitoid complexes in the southern São Francisco Craton, Brazil. Precambrian Research. 78, 151–164.

Teixeira, W. and Figueiredo, M.C.H., 1991. An outline of Early Proterozoic crustal evolution in the São Francisco region, Brazil: A review. Precambrian Research, 53(1–2), 1–22.

Terentiev, R. A & Santosh, M. 2020. Baltica (East European Craton) and Atlantica (Amazonian and West African Cratons) in the Proterozoic: The pre-Columbia connection. Earth-Science Reviews. 210, 103378.

Trouw RAJ, Peternel R, Ribeiro A, Heilbron M, Vinagre R, Duffles P, Trouw CC, Fontainha M, Kussama HH (2013). A New Interpretation for the Interference Zone between the southern Brasília belt and the central Ribeira belt, SE Brazil. Journal of South American Earth Sciences 48, 43–57.

Valeriano, C.M. 2017. The Southern Brasilia Belt. In: Heilbron M., Alkmim F., Cordani U.G. (Guest Ed.), The São Francisco Craton and its margins, Eastern Brazil. Regional Geology Review Series. Springer-Verlag, Chapter 10, 189-203.

Valeriano CM, Pimentel MM, Heilbron M, Almeida JCH, Trouw RAJ. 2008. Tectonic evolution of the Brasilia Belt, Central Brazil, and early assembly of Gondwana. Geological Society Special Publication, 294, 197–210.

Valeriano, C.M.; Machado, N.; Simonetti, A.; Valladares, C.S.; Seer, H.J.; Simões, L.S.A. 2004. U-Pb Geochronology of the Southern Brasília Belt (SE-BRAZIL):

Sedimentary Provenance, Neoproterozoic Orogeny and Assembly of West Gondwana. Precambrian Research 130, 27–55.

Vlach, S.R.F.; Campos Neto, M. C.; Caby, R.; Basei, M. A. S. 2003. Contact metamorphism in metapelites from the Nova Lima Group, Rio das Velhas Supergroup, Quadrilátero Ferrífero: a monazite Th-U-PbT dating by the electron-probe microanalyser. In: IV South American Symposium on Isotope Geology, Salvador. Short Papers, 1, 307–310.

Wang, Q., Xu, J.-F., Jian, P., Bao, Z.-W., Zhao, Z.-H., Li, C.-F., Xiong, X.-L., Ma, J.-L., 2006.Petrogenesis of adakitic porphyries in an extensional tectonic setting, Dexing,South China: implications for the genesis of porphyry copper mineralization. Journal of Petrology 47, 119–144.

Wu, G., Yang, S., Meert, J.G., Xiao, Y., Chen, Y., Wang, Z., Li, X. 2020. Two phases of Paleoproterozoic orogenesis in the Tarim Craton: Implications for Columbia assembly. Gondwana Research 83, 201-216.

Xiong X.L., Li X.H., Xu J.F., Li W.X., Zhao Z.H., Wang Q. 2003. Extremely high-Na adakite-like magmas derived from alkali-rich basaltic underplate: The Late Cretaceous Zhantang andesites in the Huichang Basin, SE China. Geochemical Journal 37(2), 233-252.

Xu H., Yang T., Dekkers M.J., Peng P., Li S., Deng C., Zhu R. 2020. Magma flow pattern of the 1.78 Ga dyke swarm of the North China Craton during the initial assembly of the Supercontinent Nuna/Columbia: Constraints from rock magnetic and anisotropy of magnetic susceptibility studies. Precambrian Research., 345, 105773.

Xu, H., Yang, Z., Peng, P., Meert, J.G., Zhu, R. 2014. Paleo-position of the North China craton within the Supercontinent Columbia: constraints from new paleomagnetic results. Precambrian Research 255, 276-293.

Xu, J., Shinjio, R., Defant, M.J., Wang, Q., Rapp, R.P., 2002. Origin of Mesozoic adakitic intrusive rocks in the Ningzhen area of east China: partial melting of delaminated lower continental crust? Geology 12, 1111–1114.

Xu, W.L., Wang, Q.H., Wang, D.Y., Guo, J.H., Pei, F.P. 2006. Mesozoic adakitic rocks from the Xuzhou–Suzhou area, eastern China: evidence for partial melting of delaminated lower continental crust. Journal of Asian Earth Science 27, 230–240.

Yakubchuk A. 2010. Restoring the supercontinent Columbia and tracing its fragments after its breakup: a new configuration and a Super Horde hypothesis Journal of Geodynamics, 50, 166-175.

Zhao G., Sun M., Wilde S.A., Li S. 2004. A Paleo-Mesoproterozoic supercontinent: assembly, growth and breakup Earth Science Review, 67, 91-123.

Zhao, G., Cawood, P.A., Wilde, S.A., Sun, M. 2002. Review of global 2.1–1.8 Ga orogens: implications for a pre-Rodinia supercontinent. Earth Science Reviews 59, 125-162.

Zincone, S, Oliveira, E., Ribeiro, B., Marinho, M. 2020. High-K granites between the Archean Gavião and Jequié blocks, São Francisco Craton, Brazil: Implications for cratonization and amalgamation of the Rhyacian Atlantica continent. Journal of South American Earth Science. https://doi.org/10.1016/j.jsames.2020.102920.

Figures Caption

Figure 1: Tectonic framework of the São Francisco Craton basement. a) South American Platform and Gondwana configuration adapted from D'Agrella-Filho & Cordani (2017). b) Archean blocks and Paleoproterozoic magmatic arcs of the São Francisco Paleocontinent. Modified from Bruno et al., 2020; Bersan et al., 2020; Degler et al., 2018; Alkmin & Teixeira, 2017; Barbosa & Barbosa, 2017.

Figure 2: a) Neoproterozoic compartmentation of the basement units associated to the São Francisco Craton; b) Geological map and compiled U-Pb data of the southern São Francisco Paleocontinent reworked during the Brasiliano/Pan-African orogeny (Modified from Bruno et al., 2020; Alkmin & Teixeira 2017; Heilbron et al., 2017; Peres et al., 2004). Compiled U-Pb data from: Bruno et al., 2020; Cardoso et al., 2019; Pinheiro et al., 2019; Moreira et al., 2018; Teixeira et al., 2015; Seixas et al., 2013; Seixas et al., 2012; Corrêa Neto et al., 2012; Heilbron et al., 2010; Ávila et al., 2014; Noce et al., 2007;; Duarte et al., 2004; Quéméneur et al., 2003; Silva et al., 2002).

Figure 3: Field photographs of representative lithologies and outcrops of the Piedade Block, Campos Gerais Complex and Mineiro Belt. a) Metric layer of amphibolite (68B) showing sharp contact with the country rock (68A - biotite gneiss) from the Piedade Block; b) Amphibolite (70A) from the Piedade Block; c) Megacrystic Biotite -Muscovite Gneiss (58A) from the Piedade Block; d) Hornblende-Biotite Gneiss (50) from the Piedade Block e) Biotite orthogneiss (48A) from the Campo Belo Complex; f) Biotite orthogneiss (48B) from the Campo Belo Complex; g) Granodioritic Hornblende-Biotite orthogneiss (51B) from the Mineiro Belt; i) Dioritic Hornblende-Biotite orthogneiss (42) from the Mineiro Belt.

Figure 4: Photomicrographs from thin sections of the studied orthogneisses and metabasic rocks of the Piedade Block. a) Sample 70B; b) Sample 70A; c) Sample 70A under crossed nicols; d) Sample 58B; e) Sample 58A; f) Sample 58A.

Figure 5: Photomicrographs from thin sections of the studied orthogneisses and metabasic rocks of the Campo Belo Complex. a) Sample 48A; b) Sample 48A; c) Sample 48B; d) Sample 48B.

Figure 6: Photomicrographs from thin sections of the studied orthogneisses of the Mineiro Belt. a) Sample 42; b) Sample 42; c) Sample 51B; d) Sample 51B.

Figure 7: a) AFM diagram of Irvine and Baragar (1971) showing the intermediate and acid samples plotting in the calc-alkaline series and the basic rocks in the tholeiite series; b) TAS classificatory diagram (SiO_2 vs. Na_2O+K_2O) of Cox (1979).

Figure 8: a) A/NK vs. A/CNK diagram (after Shand, 1943); b) SiO_2 vs. K_2O diagram (Peccerillo & Taylor, 1976); c) FeOt / (FeOt + MgO) vs. SiO_2 (Frost et al., 2001); d) Ternary classification diagram from Laurent et al. (2014). Vertices are: 2 × A/CNK (molar $Al_2O_3/(CaO + K_2O + Na_2O)$ ratio); Na_2O/K_2O and 2 × (FeO_t + MgO) × (Sr + Ba) wt.% (=FMSB).

Figure 9: : Left column (a) TTG Sample; c) Sanukitoid Group; e) Biotite- Two-Mica Group; g) Hybrid Granitoid Group, i) Alkaline Sample): Average chondrite-normalized REE patterns normalized after values from Boynton (1984); Right column (b) TTG Sample; d) Sanukitoid Group; f) Biotite- Two-Mica Group; h) Hybrid Granitoid Group, j) Alkaline Sample): Mantle-normalized multielement plots (McDonough and Sun, 1995).

Figure 10: a) Average chondrite-normalized REE patterns normalized after values from Boynton (1984); b) NMORB-normalized multielement plot (Sun & McDonough, 1989); c) Ternary Diagram Zr/4 vs. 2Nb vs. Y of Meschede (1986); d) Tectonic discriminant diagram Zr vs. Ti (Pearce, 1982).

Figure 11: Concordia diagrams presenting zircon U-Pb results and Cathodoluminescence (CL) and Backscattered electrons (BSE) images of representative zircon grains for the rocks of the Piedade Block. Circles on the zircon grains indicate spot locations for U-Pb results. Paleoproterozoic and Archean data are shown in $^{207}Pb/^{206}Pb$ and Neoproterozoic data in $^{206}Pb/^{238}U$. Zircon codes refer to analytical ID in U-Pb data table in Supplementary Material C. Blue circles are indicative of inherited zircon grains. a) Two Discordia lines for Sample 50. Inset of Paleoproterozoic sub concordant rims; b) Concordia age for the Neoproterozoic metamorphic overprint of Sample 50; c) Concordia age for the Archean crystallization age of Sample 50; d) Sample 65; e) Sample 68A, inset of Concordia age for crystallization; f) Sample 70A, inset of Concordia age for crystallization; g) Sample 70B, inset of Concordia age for crystallization.

Figure 12: Concordia diagrams presenting zircon U-Pb results and Cathodoluminescence (CL) and Backscattered electrons (BSE) images of representative zircon grains for the rocks of the Piedade Block. Circles on the zircon grains indicate spot locations for U-Pb results. Paleoproterozoic and Archean data are shown in $^{207}Pb/^{206}Pb$ and Neoproterozoic data in $^{206}Pb/^{238}U$. Zircon codes refer to analytical ID in U-Pb data table in Supplementary Material C. a) Sample 58A, inset of Paleoproterozoic Average Mean of the analytical results; b) Sample 58B.

Figure 13: Concordia diagrams presenting zircon U-Pb results and Cathodoluminescence (CL) and Backscattered electrons (BSE) images of representative zircon grains for the rocks of the Mineiro Belt. Circles on the zircon grains indicate spot locations for U-Pb results. Paleoproterozoic and Archean data are shown in $^{207}Pb/^{206}Pb$ and Neoproterozoic data in $^{206}Pb/^{238}U$. Zircon codes refer to analytical ID in U-Pb data table in Supplementary Material C. Blue circles are indicative of inherited zircon grains. a) Sample 42; b) Average Mean of Sample 42 results; c) Sample 51B; d) Sample 52B.

Figure 14: Concordia diagrams presenting zircon U-Pb results and Cathodoluminescence (CL) and Backscattered electrons (BSE) images of representative zircon grains for the rocks of the Campo Belo Complex. Circles on the zircon grains indicate spot locations for U-Pb results. Paleoproterozoic and Archean data are shown in $^{207}Pb/^{206}Pb$ and Neoproterozoic data in $^{206}Pb/^{238}U$. Zircon codes refer to analytical ID in U-Pb data table in Supplementary Material C. Blue circles are indicative of inherited zircon grains. a) Sample 48A, inset for concordia age; b) Sample 48B.

Figure 15: Nd evolution vs time (crystallization ages) diagram. DM model from De Paolo, 1981. Different symbols for tectono-stratigraphic terranes and different colors for the lithogeochemical groups.

Figure 16: Isotopic diagram for the Campo Belo Complex, Mineiro Belt and Piedade Block samples. εNd vs initial $^{87}Sr/^{86}Sr$ diagram (Sr and Nd isotopic systematics of the crust and mantle, horizontal grey band is the estimated εNd of the bulk silicate of Caro and Bourdon (2010); vertical grey band between dashed lines in their estimated bulk silicate Earth $^{87}Sr/^{86}Sr$)

Figure 17: Binary plots of isotopic signatures. #mg vs. a) εNd (crystallization ages)/ b) $^{87}Sr/^{86}Sr$ (initial); c) Plot of incompatible element (Sr+Ba ppm) vs. FeOt + MgO (wt.)

(Laurent et. al., 2014); d) $Na_2O + K_2O$+ FeOt + MgO + TiO_2-($Na_2O + K_2O$) / (FeOt + MgO + TiO_2) diagram (from PatiñoDouce, 1999).

Figure 18: Table of synthetized results of this study (*) within the Minas segment of the São Francisco Paleocontinent (Bruno et. al., 2020; Cutts, et. al., 2020; Araújo et. al., 2019b; Cutts et. al., 2019; Moreira, et. al., 2018; Degler et. al., 2018; Alkmim & Teixeira, et. al., 2017; eg. Heilbron et. al., 2017b, eg. Teixeira et. al., 2017a, eg. Albert et. al., 2016; Teixeira et. al., 2015, Aguilar Gil et. al., 2015; Farina et. al., 2015; Seixas et. al., 2013; Noce et. al., 2007; Vlach et. al., 2003; Silva et. al., 2002; Brueckner et. al., 2000; Machado et. al., 1992).

Figure 19: Integrated tectonic evolution model for the Minas segment of the Paleoproterozoic Orogeny, southeast Brazil, as envisaged for the period between ca. 2.4 and 1.9 Ga (Modified after Bruno et. al., 2020; Cutts et. al., 2020; Ávila et. al., 2014; Heilbron et. al., 2010; Noce et. al., 2007)

Figure 20: a) Paleotectonic framework of the Sao Francisco Paleocontinent at ca. 2.2 Ga, distinguished by individual Archean blocks and Paleoproterozoic accretionary orogenic belt and envisaged tectonic model for the Bahia segment (A-A') and the Minas segment (B-B') of the Minas Bahia Orogenic Belt (modified from Zincone et. al., 2020; Teixeira et. al., 2017a; Alkmim & Noce, 2006). UAC – Undivided Archean Complexes (e.g. Campo Belo, Belo Horizonte, Bonfim, Santa Bárbara); b) εNd vs. εSr diagram with distinct fields characterized by data from the Itabuna-Salvador-Curaçá Belt, Gavião, Serrinha and Jequié block (modified after Barbosa and Barbosa, 2017), Mantiqueira Complex (Bruno et. al., 2020); Piedade Block (Bruno et. al., 2020 and from this study); Mineiro Belt (Cardoso et. al., 2019; Teixeira et. al., 2015 and this study) and Juiz de Fora Complex (Araújo et. al., 2019b).

Figure 21: a) Paleogeographic reconstruction at ca. 2.0 Ga (D'Agrella-Filho & Cordani, 2017). Su – Superior Craton; S – Slave Craton; R – Rae cratonic fragment; H – Hearne cratonic fragment. KAR – Karelia Craton; K – Kola Craton; Pam – Proto-Amazonia; WA - West Africa; V-U – Volgo Uralia; AS – Sarmatia; CSF – Congo/São Francisco; KAL – Kalahari; RP – Rio de La Plata; BTS – Borborema Trans-Sahara. Dashed lines indicate later borders of Laurentia, Baltica and Amazonian craton; b) Paleogeographic reconstruction of Columbia Supercontinent at ca. 1.78 Ga (D'Agrella-Filho et. al., 2020). AC- Amazonia Craton; WA – West African Craton; BA – Baltica Craton; LA – Laurentia Craton; SIB – Siberia Craton; IN – India Craton; NC – North China Craton; LP – Rio de La Plata Craton; SF – São Francisco Craton; C – Congo Craton; NAU – North Australia Craton; EA – East Antarctica; SAU – South Australia Craton; WAU – Western Australia Craton.

Figures

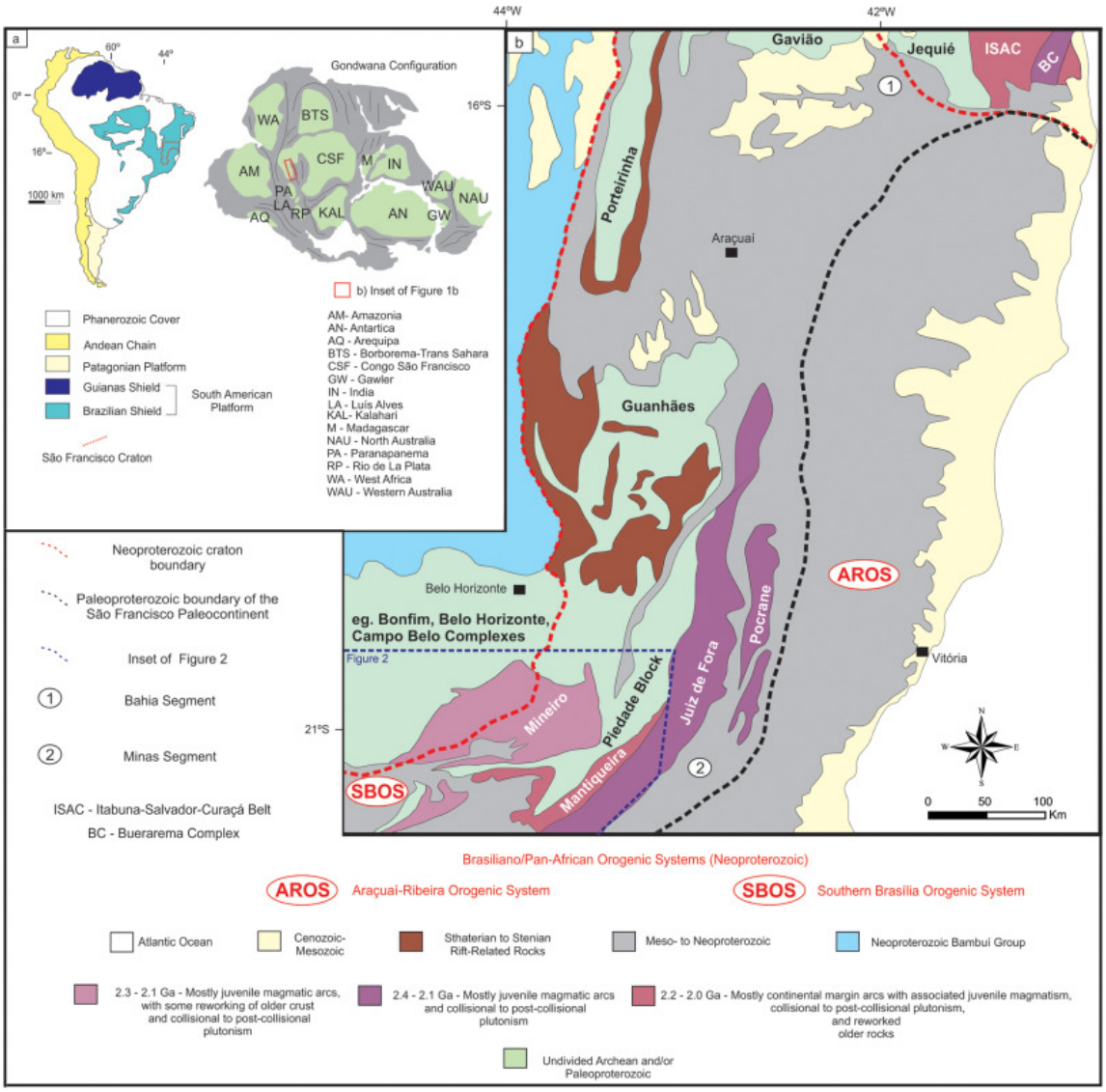

Figure 1

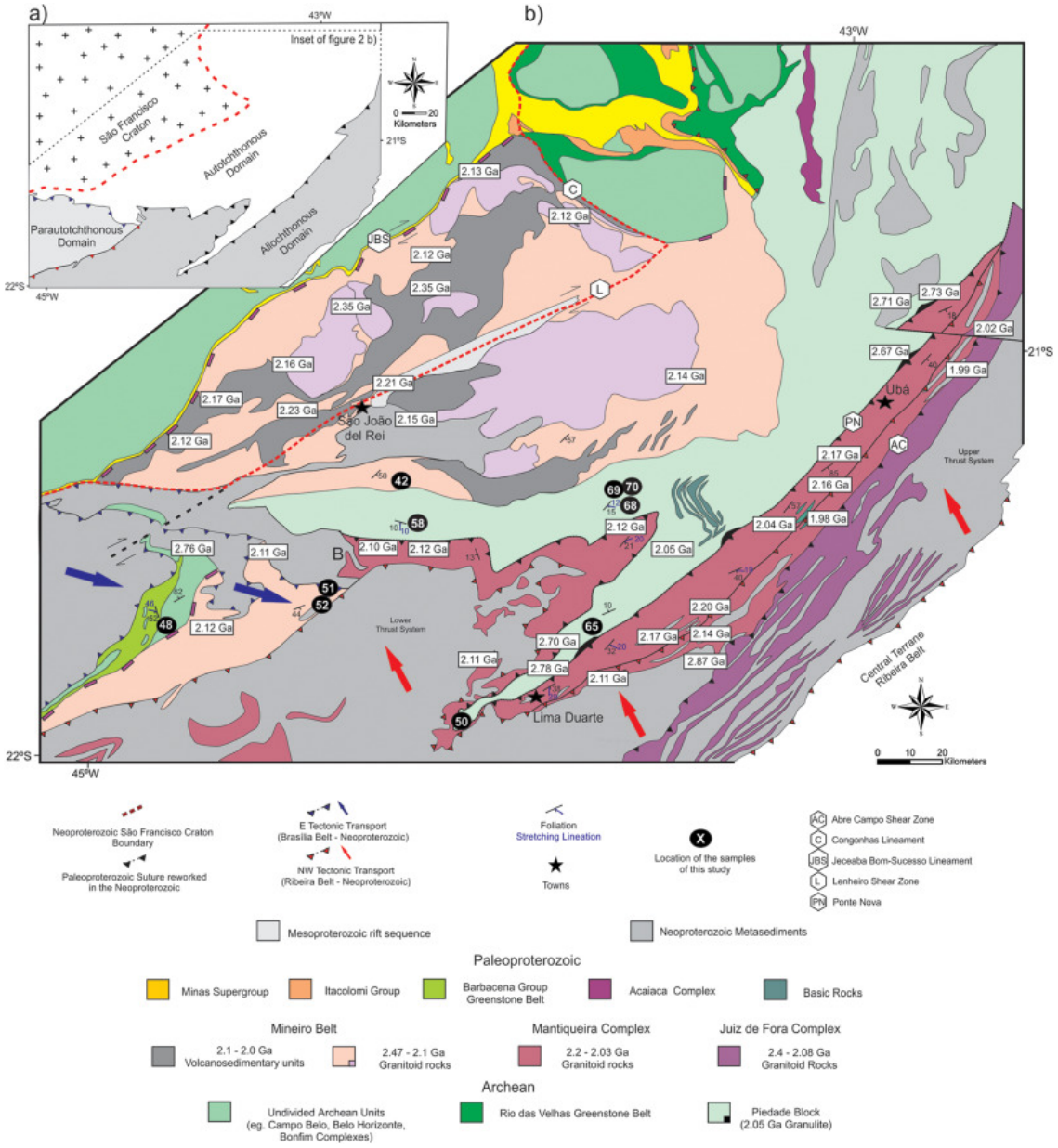
a)
b)
Inset of figure 2 b)
São Francisco Craton
Autochthonous Domain
Parautotchthonous Domain
Allochthonous Domain
0 20 Kilometers
43°W
45°W
22°S
21°S
São João del Rei
Ubá
Lima Duarte
Lower Thrust System
Upper Thrust System
Central Terrane Ribeira Belt
0 10 20 Kilometers
Neoproterozoic São Francisco Craton Boundary
Paleoproterozoic Suture reworked in the Neoproterozoic
E Tectonic Transport (Brasília Belt - Neoproterozoic)
NW Tectonic Transport (Ribeira Belt - Neoproterozoic)
Foliation
Stretching Lineation
Towns
Location of the samples of this study
Abre Campo Shear Zone
Congonhas Lineament
Jeceaba Bom-Sucesso Lineament
Lenheiro Shear Zone
Ponte Nova
Mesoproterozoic rift sequence
Neoproterozoic Metasediments
Paleoproterozoic
Minas Supergroup
Itacolomi Group
Barbacena Group Greenstone Belt
Acaiaca Complex
Basic Rocks
Mineiro Belt
2.1 - 2.0 Ga Volcanosedimentary units
2.47 - 2.1 Ga Granitoid rocks
Mantiqueira Complex
2.2 - 2.03 Ga Granitoid rocks
Juiz de Fora Complex
2.4 - 2.08 Ga Granitoid Rocks
Archean
Undivided Archean Units (eg. Campo Belo, Belo Horizonte, Bonfim Complexes)
Rio das Velhas Greenstone Belt
Piedade Block (2.05 Ga Granulite)

Figure 2

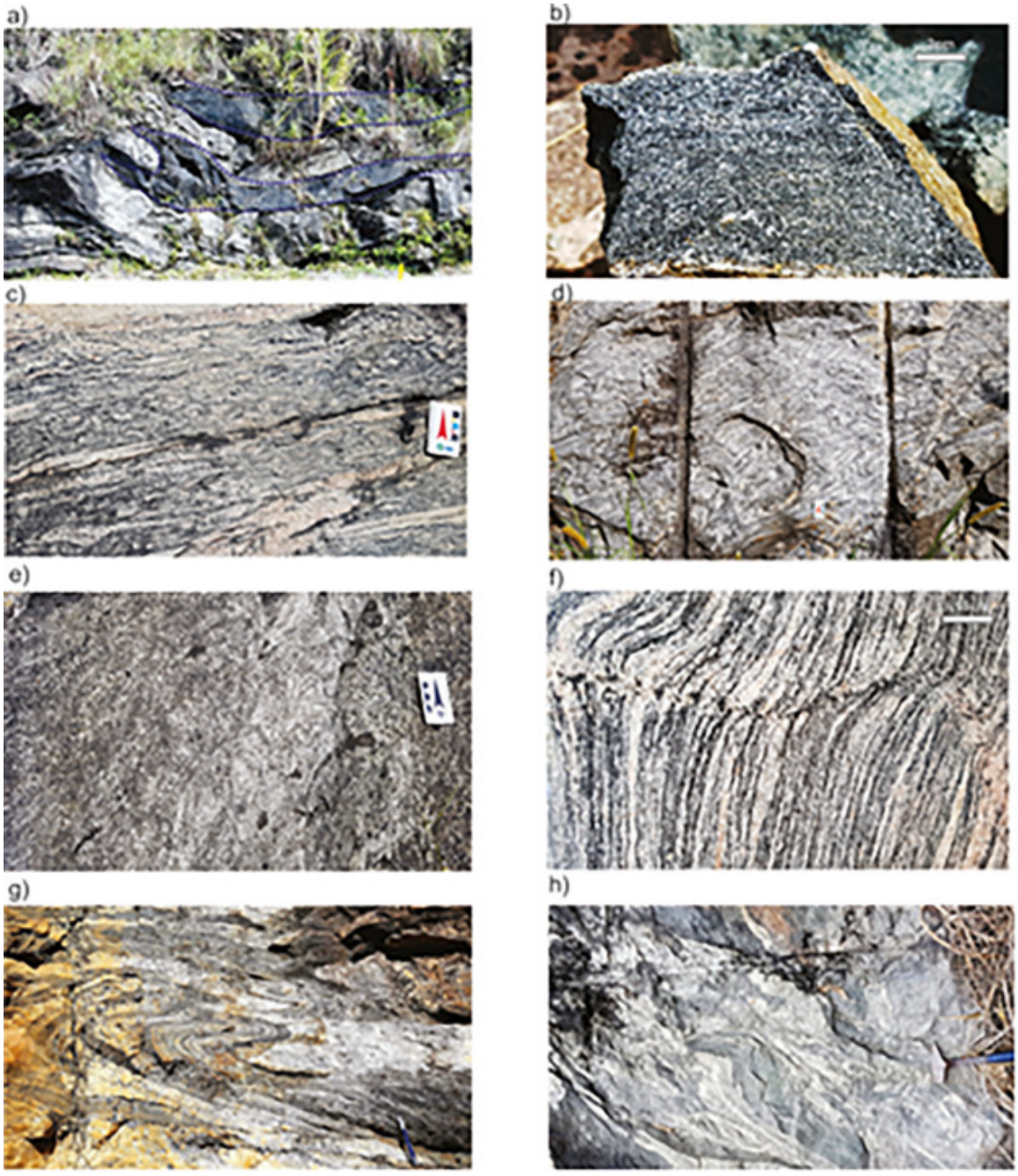

Figure 3

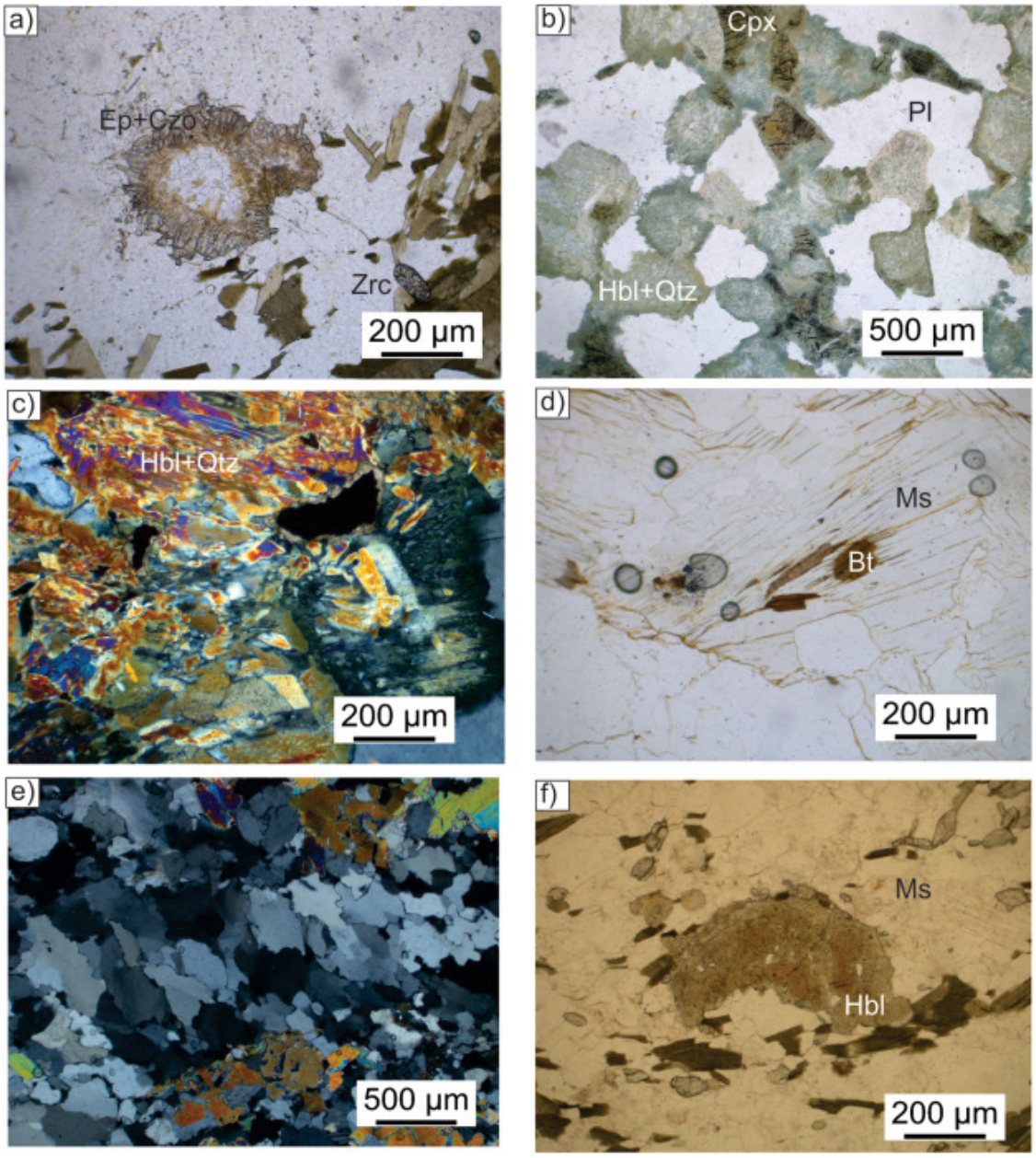
a)
Ep+Czo
Zrc
200 µm
b)
Cpx
Pl
Hbl+Qtz
500 µm
c)
Hbl+Qtz
200 µm
d)
Ms
Bt
200 µm
e)
500 µm
f)
Ms
Hbl
200 µm

Figure 4

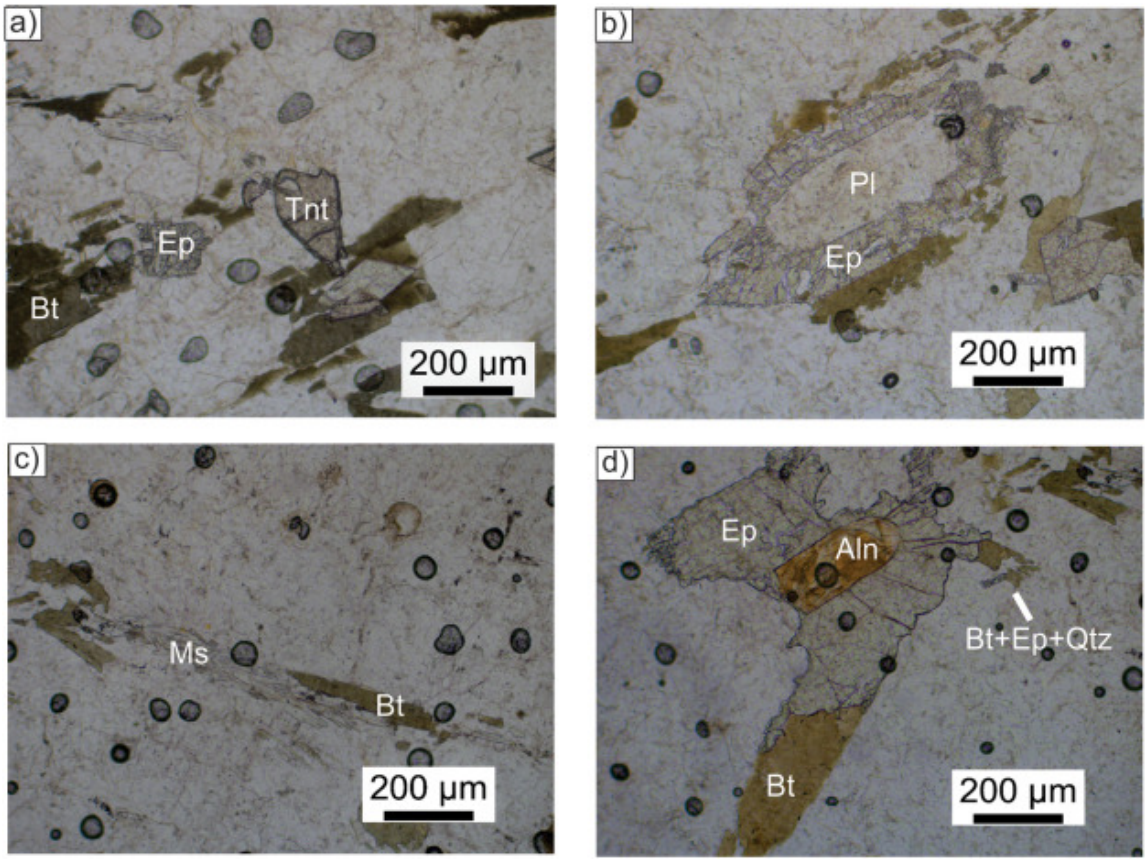

Figure 5

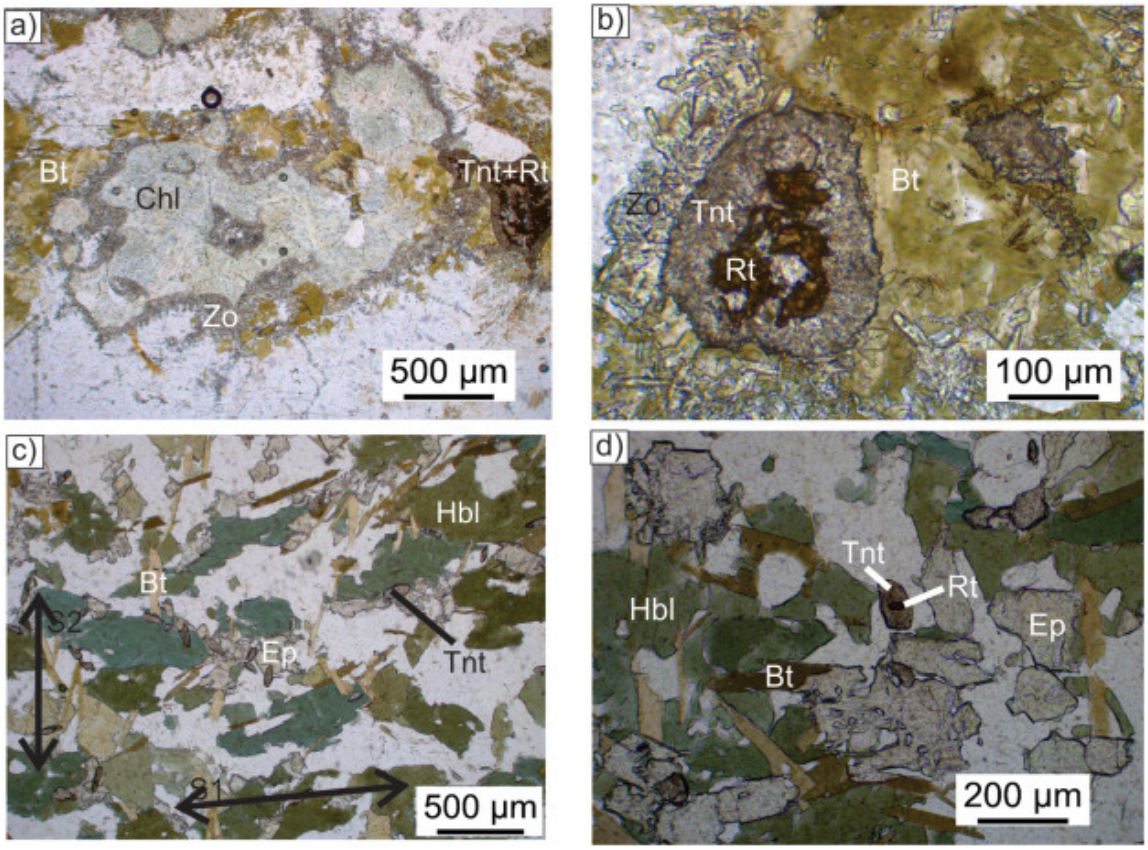

Figure 6

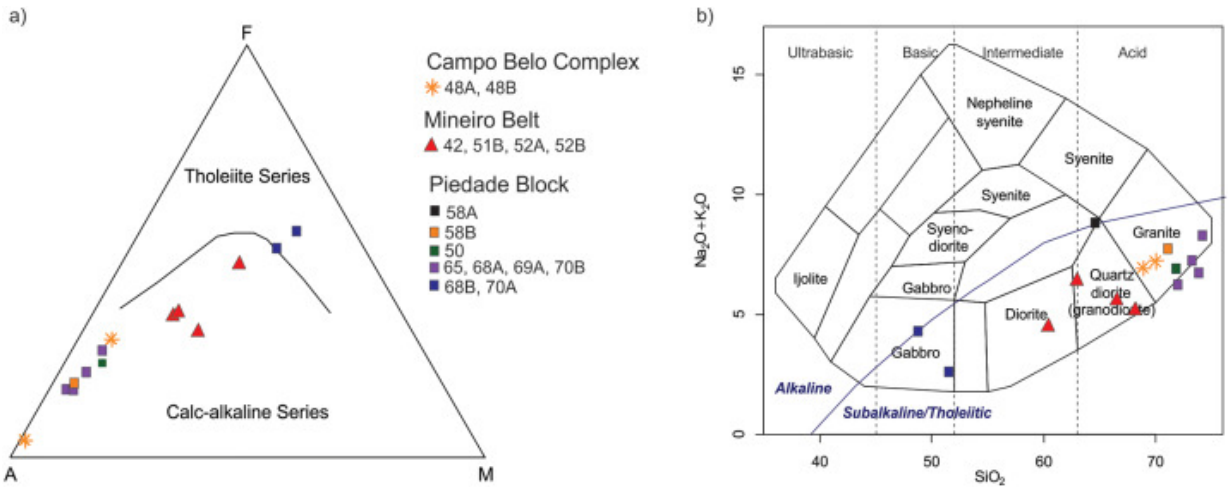

Figure 7

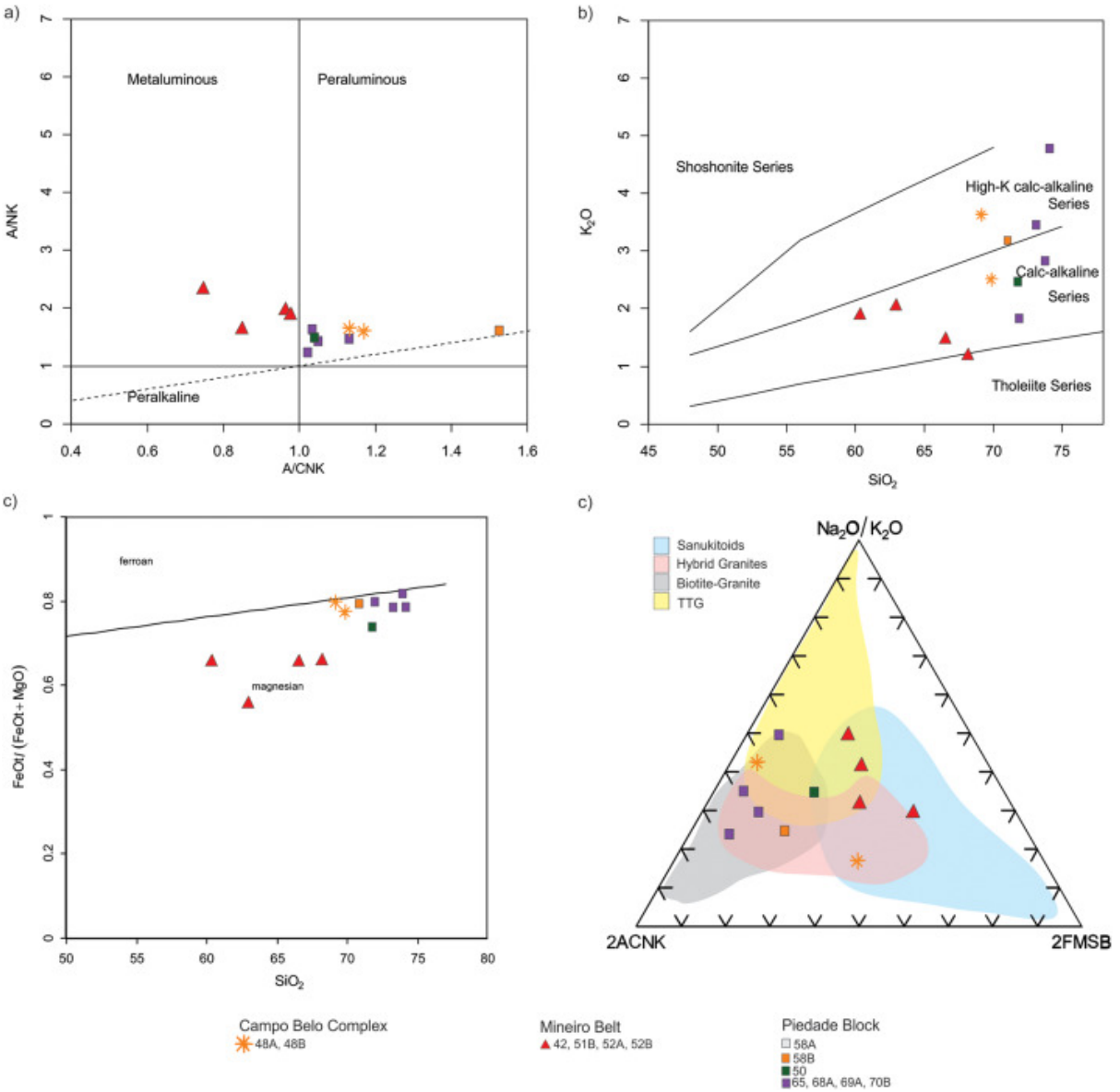

Figure 8

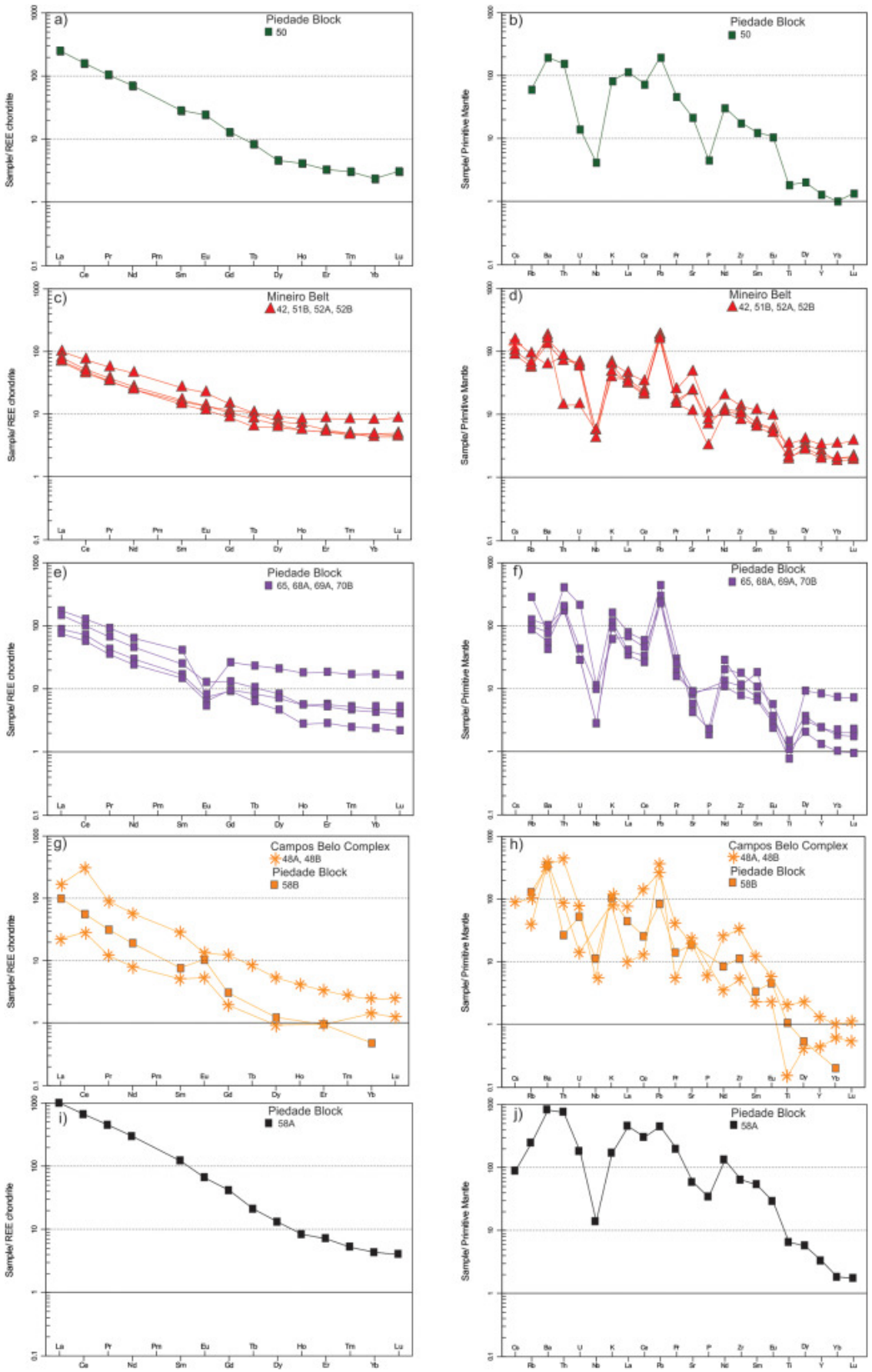
a)
Piedade Block
50
Sample/ REE chondrite
b)
Piedade Block
50
Sample/ Primitive Mantle
c)
Mineiro Belt
42, 51B, 52A, 52B
Sample/ REE chondrite
d)
Mineiro Belt
42, 51B, 52A, 52B
Sample/ Primitive Mantle
e)
Piedade Block
65, 68A, 69A, 70B
Sample/ REE chondrite
f)
Piedade Block
65, 68A, 69A, 70B
Sample/ Primitive Mantle
g)
Campos Belo Complex
48A, 48B
Piedade Block
58B
Sample/ REE chondrite
h)
Campos Belo Complex
48A, 48B
Piedade Block
58B
Sample/ Primitive Mantle
i)
Piedade Block
58A
Sample/ REE chondrite
j)
Piedade Block
58A
Sample/ Primitive Mantle

Figure 9

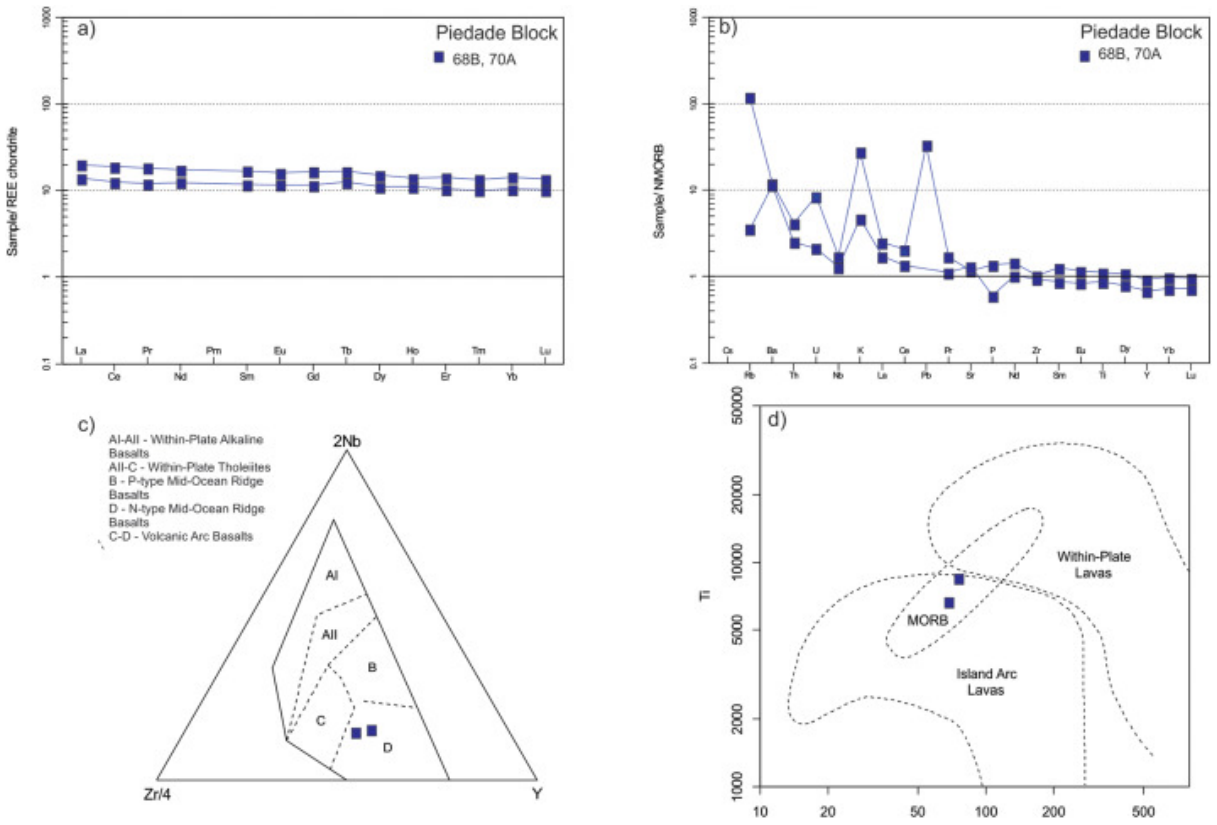
a)
Piedade Block
68B, 70A
Sample/ REE chondrite
La
Ce
Pr
Nd
Pm
Sm
Eu
Gd
Tb
Dy
Ho
Er
Tm
Yb
Lu
b)
Piedade Block
68B, 70A
Sample/ NMORB
c)
AI-AII - Within-Plate Alkaline Basalts
AII-C - Within-Plate Tholeiites
B - P-type Mid-Ocean Ridge Basalts
D - N-type Mid-Ocean Ridge Basalts
C-D - Volcanic Arc Basalts
2Nb
Zr/4
Y
AI
AII
B
C
D
d)
Ti
Within-Plate Lavas
MORB
Island Arc Lavas

Figure 10

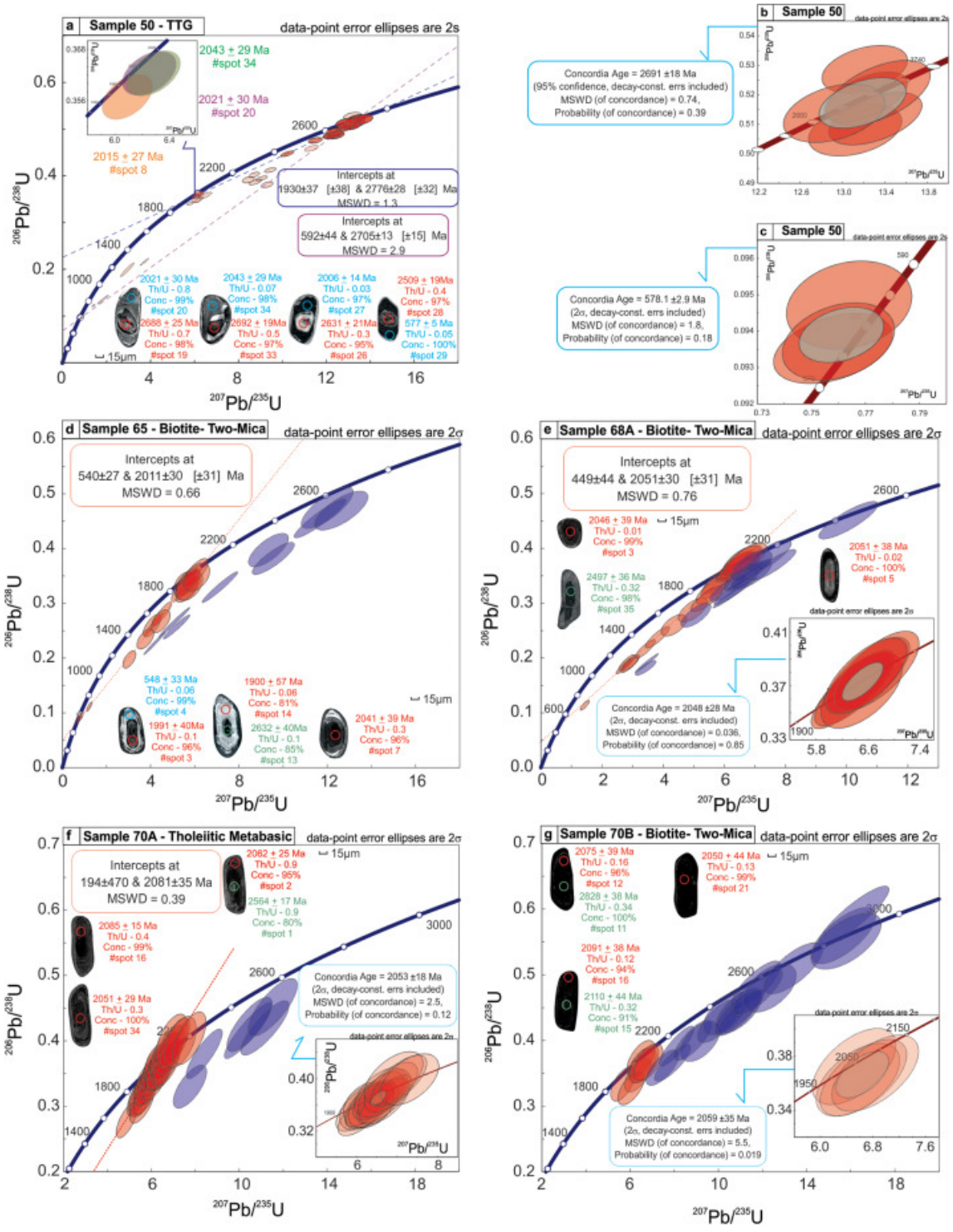
a Sample 50 - TTG
data-point error ellipses are 2s
2043 ± 29 Ma
#spot 34
2021 ± 30 Ma
#spot 20
2015 ± 27 Ma
#spot 8
Intercepts at
1930±37 [±38] & 2776±28 [±32] Ma
MSWD = 1.3
Intercepts at
592±44 & 2705±13 [±15] Ma
MSWD = 2.9
2021 ± 30 Ma Th/U - 0.8 Conc - 99% #spot 20
2688 ± 25 Ma Th/U - 0.7 Conc - 98% #spot 19
2043 ± 29 Ma Th/U - 0.07 Conc - 98% #spot 34
2692 ± 19Ma Th/U - 0.5 Conc - 97% #spot 33
2006 ± 14 Ma Th/U - 0.03 Conc - 97% #spot 27
2631 ± 21Ma Th/U - 0.3 Conc - 95% #spot 26
2509 ± 19Ma Th/U - 0.4 Conc - 97% #spot 28
577 ± 5 Ma Th/U - 0.05 Conc - 100% #spot 29
15µm
206Pb/238U
207Pb/235U
b Sample 50
Concordia Age = 2691 ±18 Ma
(95% confidence, decay-const. errs included)
MSWD (of concordance) = 0.74,
Probability (of concordance) = 0.39
c Sample 50
Concordia Age = 578.1 ±2.9 Ma
(2σ, decay-const. errs included)
MSWD (of concordance) = 1.8,
Probability (of concordance) = 0.18
d Sample 65 - Biotite- Two-Mica
data-point error ellipses are 2σ
Intercepts at
540±27 & 2011±30 [±31] Ma
MSWD = 0.66
548 ± 33 Ma Th/U - 0.06 Conc - 99% #spot 4
1991 ± 40Ma Th/U - 0.1 Conc - 96% #spot 3
1900 ± 57 Ma Th/U - 0.06 Conc - 81% #spot 14
2632 ± 40Ma Th/U - 0.1 Conc - 85% #spot 13
2041 ± 39 Ma Th/U - 0.3 Conc - 96% #spot 7
15µm
e Sample 68A - Biotite- Two-Mica
data-point error ellipses are 2σ
Intercepts at
449±44 & 2051±30 [±31] Ma
MSWD = 0.76
2046 ± 39 Ma Th/U - 0.01 Conc - 99% #spot 3
2497 ± 36 Ma Th/U - 0.32 Conc - 98% #spot 35
2051 ± 38 Ma Th/U - 0.02 Conc - 100% #spot 5
15µm
Concordia Age = 2048 ±28 Ma
(2σ, decay-const. errs included)
MSWD (of concordance) = 0.036,
Probability (of concordance) = 0.85
f Sample 70A - Tholeiitic Metabasic
data-point error ellipses are 2σ
Intercepts at
194±470 & 2081±35 Ma
MSWD = 0.39
2062 ± 25 Ma Th/U - 0.8 Conc - 95% #spot 2
2564 ± 17 Ma Th/U - 0.9 Conc - 80% #spot 1
2085 ± 15 Ma Th/U - 0.4 Conc - 99% #spot 16
2051 ± 29 Ma Th/U - 0.3 Conc - 100% #spot 34
15µm
Concordia Age = 2053 ±18 Ma
(2σ, decay-const. errs included)
MSWD (of concordance) = 2.5,
Probability (of concordance) = 0.12
g Sample 70B - Biotite- Two-Mica
data-point error ellipses are 2σ
2075 ± 39 Ma Th/U - 0.16 Conc - 96% #spot 12
2828 ± 38 Ma Th/U - 0.34 Conc - 100% #spot 11
2050 ± 44 Ma Th/U - 0.13 Conc - 99% #spot 21
2091 ± 38 Ma Th/U - 0.12 Conc - 94% #spot 16
2110 ± 44 Ma Th/U - 0.32 Conc - 91% #spot 15
15µm
Concordia Age = 2059 ±35 Ma
(2σ, decay-const. errs included)
MSWD (of concordance) = 5.5,
Probability (of concordance) = 0.019

Figure 11

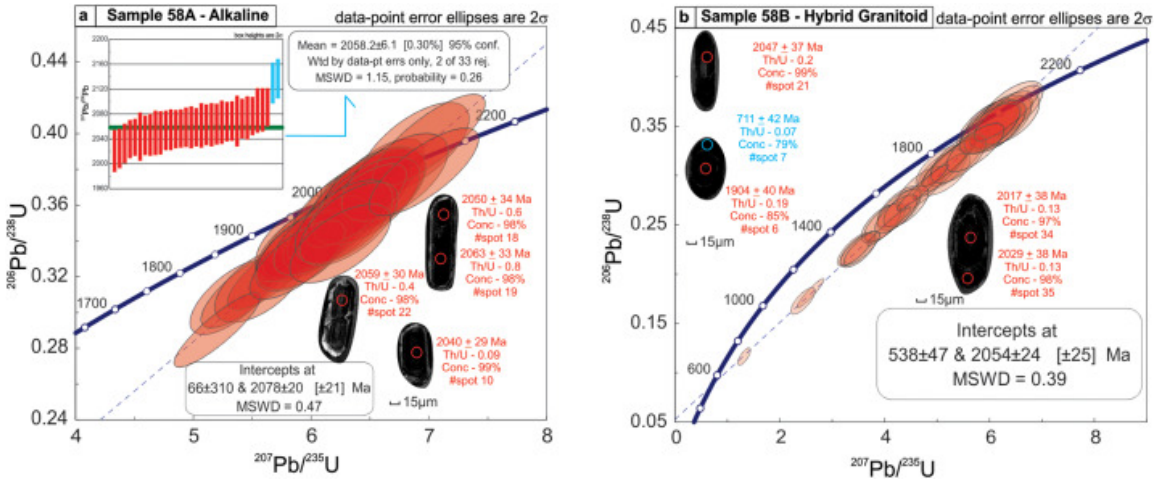

Figure 12

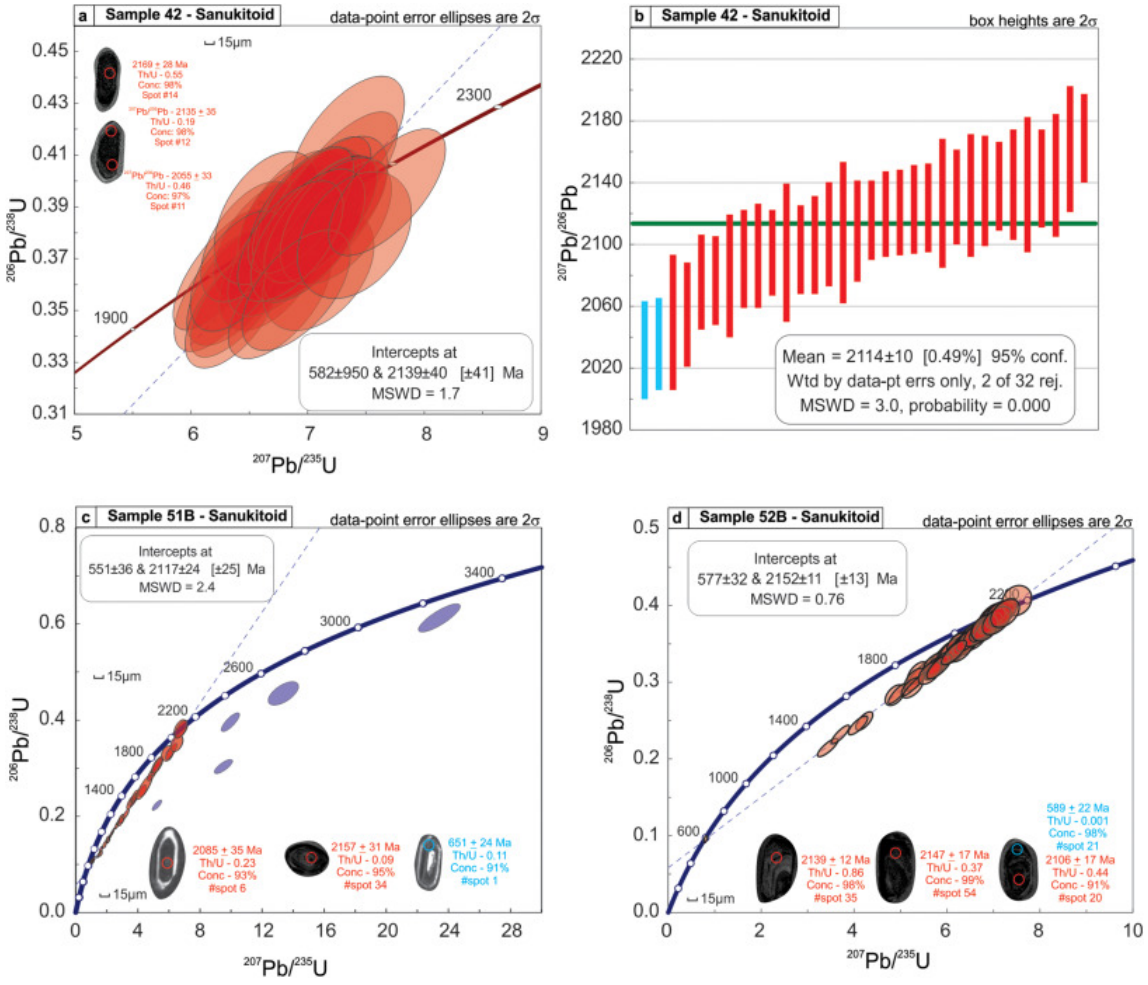

Figure 13

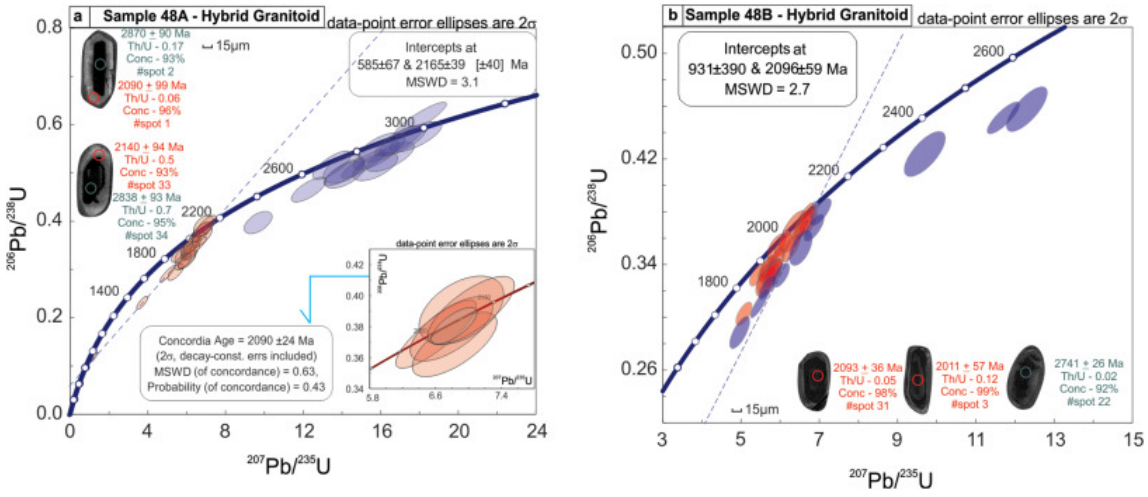

Figure 14

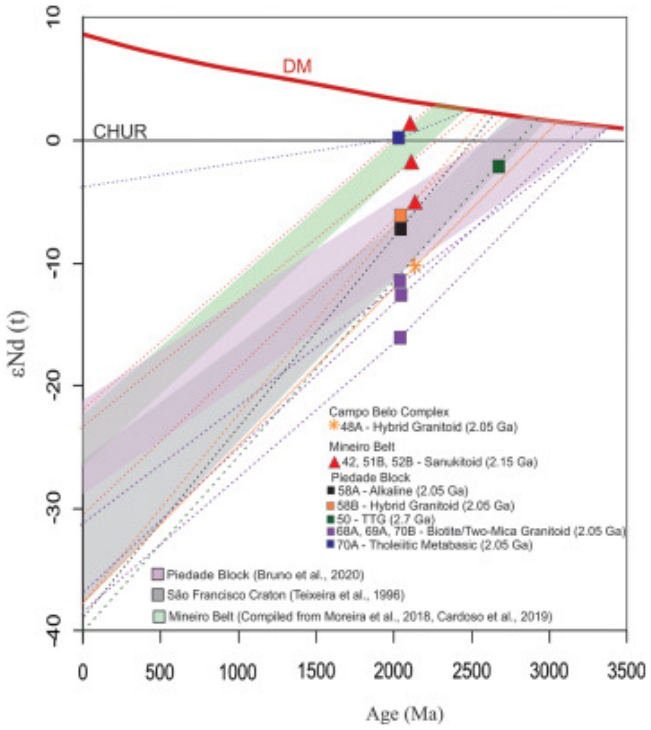

Figure 15

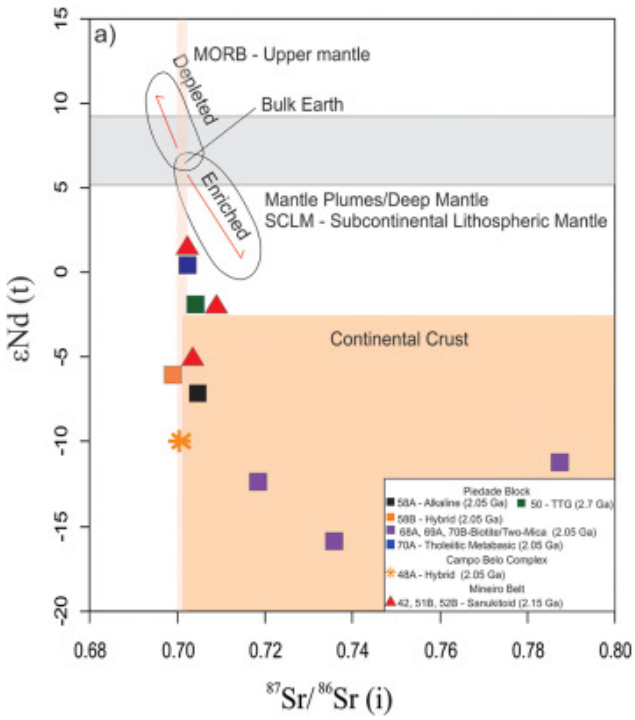

Figure 16

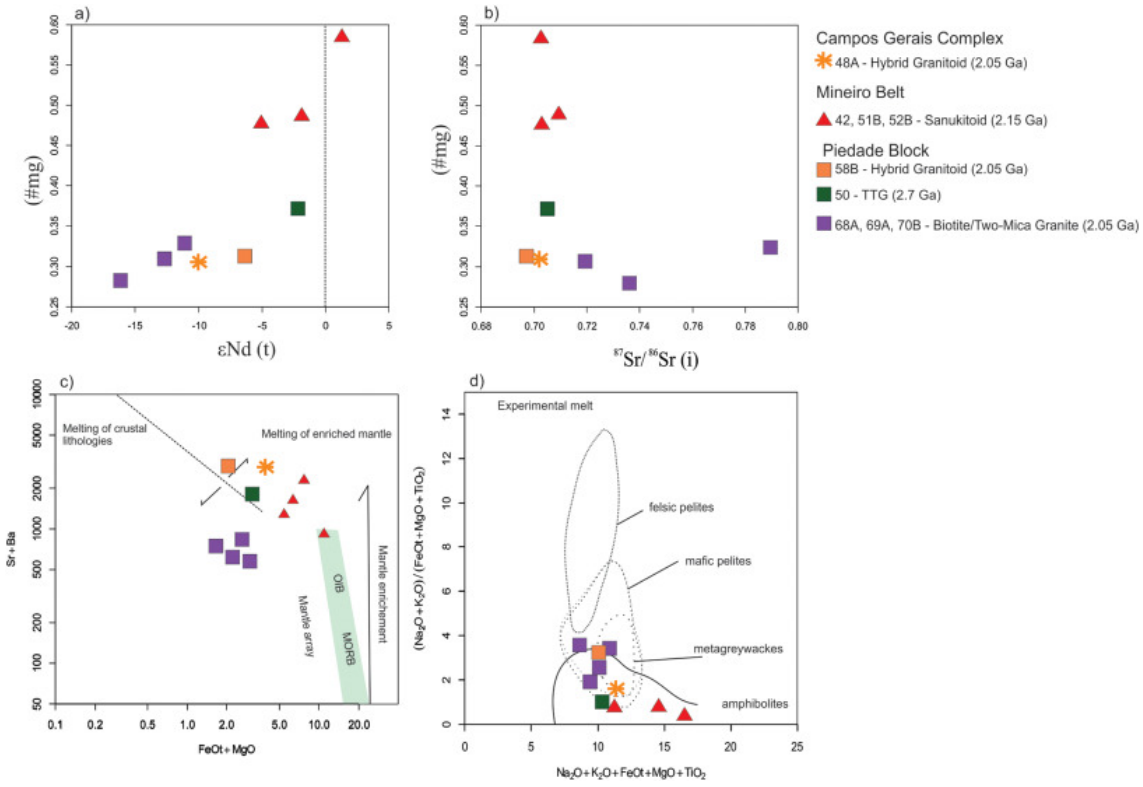

Figure 17

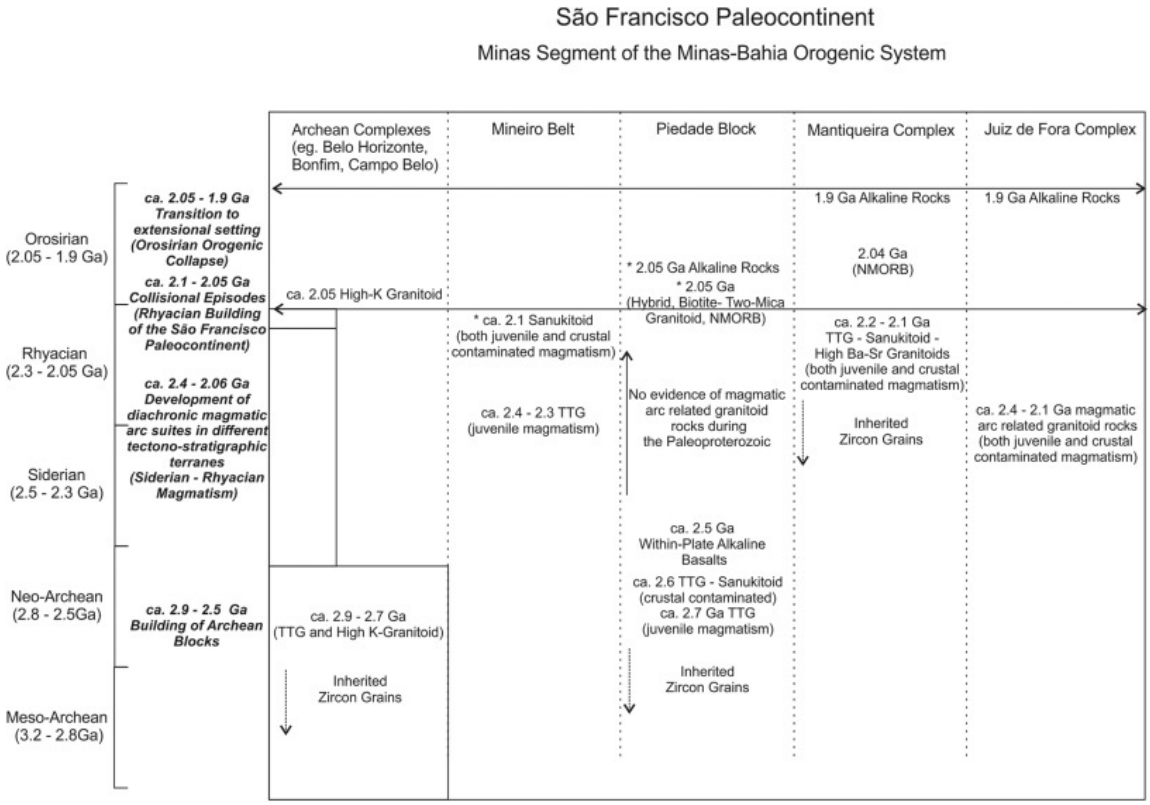

Figure 18

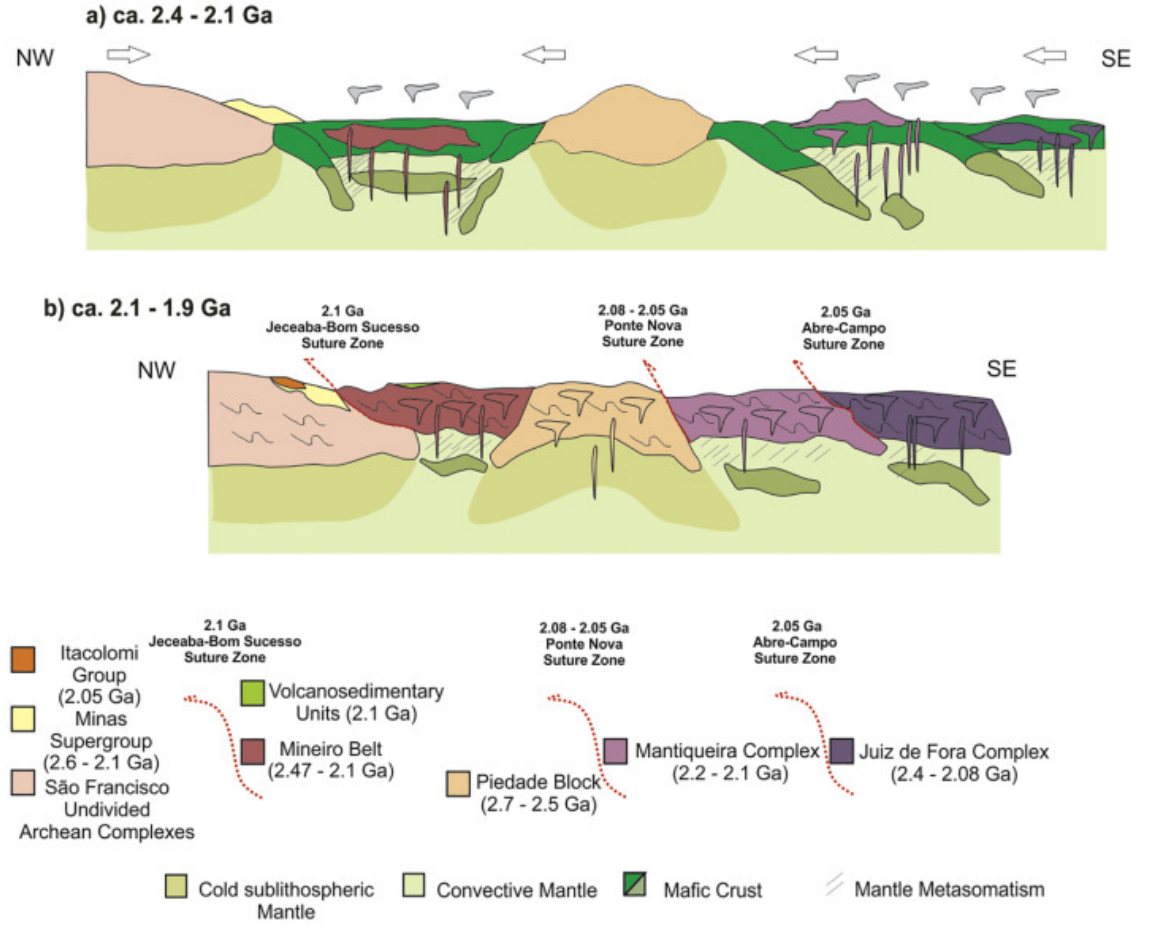

Figure 19

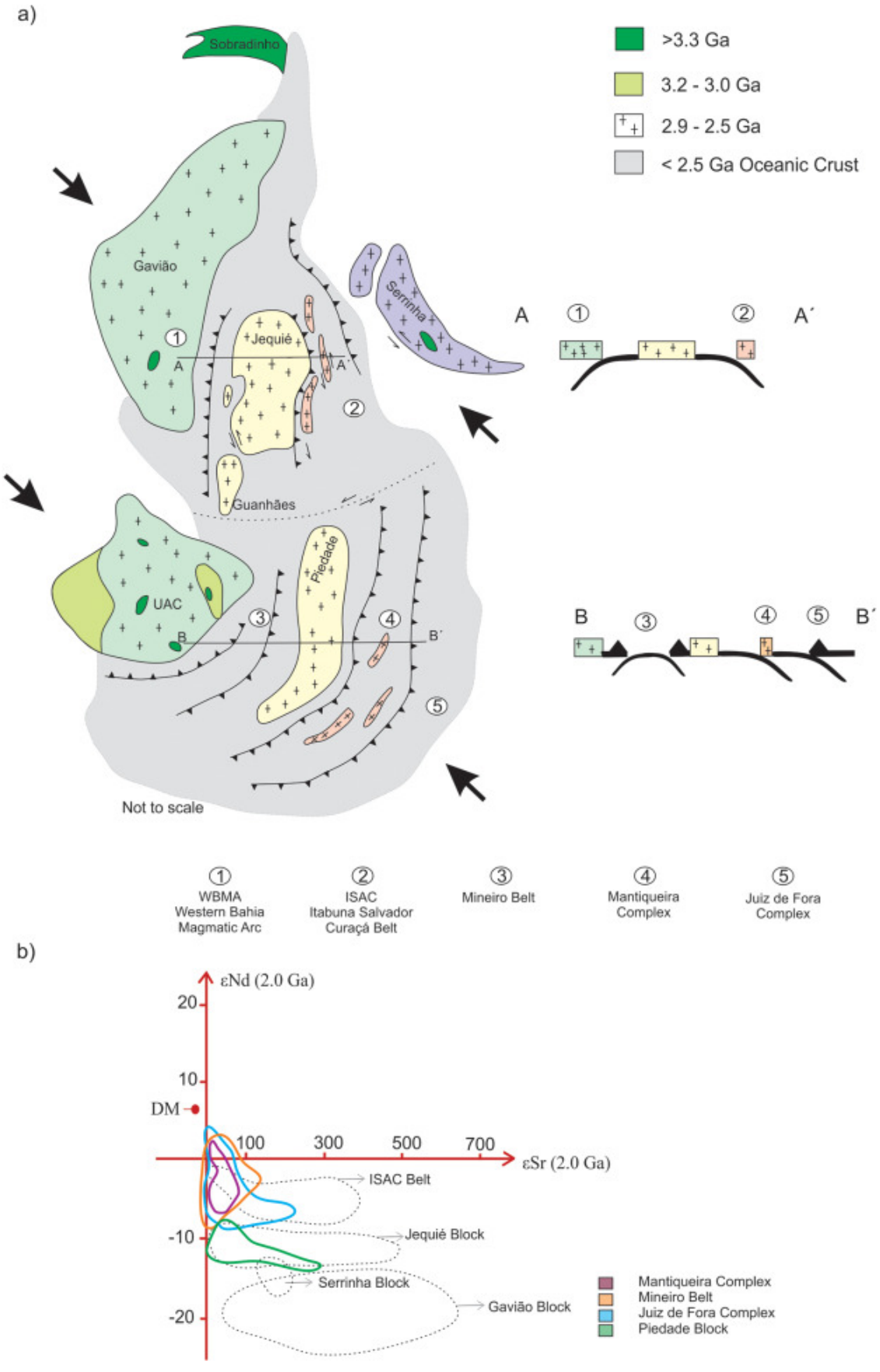
a)
>3.3 Ga
3.2 - 3.0 Ga
2.9 - 2.5 Ga
< 2.5 Ga Oceanic Crust
Sobradinho
Gavião
Jequié
Serrinha
Guanhães
Piedade
UAC
A
A´
B
B´
Not to scale
① WBMA Western Bahia Magmatic Arc
② ISAC Itabuna Salvador Curaçá Belt
③ Mineiro Belt
④ Mantiqueira Complex
⑤ Juiz de Fora Complex
b)
εNd (2.0 Ga)
20
10
DM
100
300
500
700
εSr (2.0 Ga)
ISAC Belt
Jequié Block
Serrinha Block
Gavião Block
-10
-20
Mantiqueira Complex
Mineiro Belt
Juiz de Fora Complex
Piedade Block

Figure 20

a)

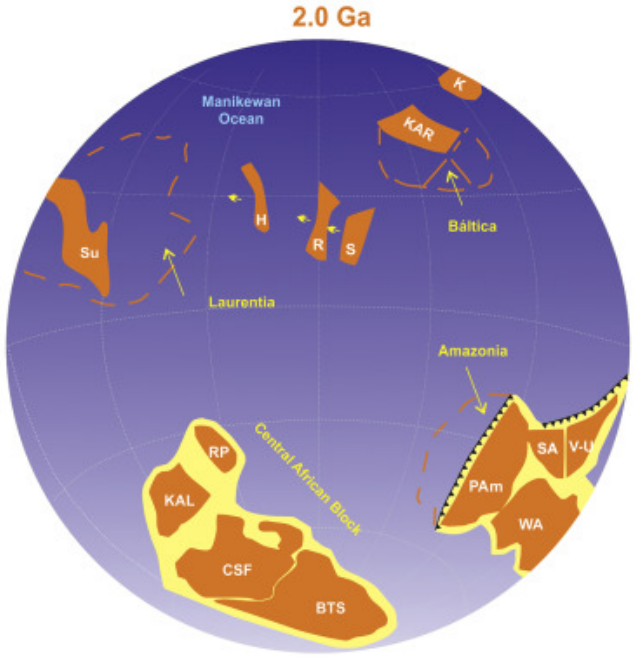
2.0 Ga
Manikewan
Ocean
K
KAR
Báltica
H
R
S
Su
Laurentia
Amazonia
RP
KAL
Central African Block
CSF
BTS
SA
V-U
PAm
WA

b)


1.78 Ga
LA
EA
SAU
WAU
SAU
C
BA
SIB
LP
SF
NC
AC
WA
IN

Figure 21